Title:

Brain composition in *Heliconius* butterflies, post-eclosion growth and experience dependent neuropil plasticity

Authors:

Stephen H. Montgomery[1], Richard M. Merrill[2,3], Swidbert R. Ott[4]

Institutional affiliations:

[1] Dept. Genetics, Evolution & Environment, University College London, Gower Street, London, UK, WC1E 6BT

[2] Dept. Zoology, University of Cambridge, Downing Street, Cambridge, UK, CB2 3EJ

[3] Smithsonian Tropical Research Institute, MRC 0580-12, Unit 9100 Box 0948, DPO AA 34002-9998, Panama

[4] Dept. Neuroscience, Psychology and Behaviour, University of Leicester, Adrian Building, University Road, Leicester, UK, LE1 7RH

Corresponding author: Stephen H. Montgomery: Stephen.Montgomery@cantab.net

Running head: *Anatomy and plasticity of* Heliconius *brains*

Key words: adaptive brain evolution, comparative neuroanatomy, *Heliconius*, Lepidoptera, mushroom bodies, plasticity

Financial support: This research was supported by research fellowships from the Royal Commission of the Exhibition of 1851 and Leverhulme Trust, a Royal Society Research Grant (RG110466) and a British Ecological Society Early Career Project Grant awarded to SHM. RMM was supported by a Junior Research Fellowship from King's College, Cambridge and an Ernyst Mayr Fellowship from STRI. SRO was supported by a University Research Fellowship from the Royal Society, London (UK).

ABSTRACT

Behavioral and sensory adaptations are often based in the differential expansion of brain components. These volumetric differences represent changes in investment, processing capacity and/or connectivity, and can be used to investigate functional and evolutionary relationships between different brain regions, and between brain composition and behavioral ecology. Here, we describe the brain composition of two species of *Heliconius* butterflies, a long-standing study system for investigating ecological adaptation and speciation. We confirm a previous report of striking mushroom body expansion, and explore patterns of post-eclosion growth and experience-dependent plasticity in neural development. This analysis uncovers age- and experience-dependent post-emergence mushroom body growth comparable to that in foraging hymenoptera, but also identifies plasticity in several other neuropil. An interspecific analysis indicates that *Heliconius* display remarkable levels of investment in mushroom bodies for a lepidopteran, and indeed rank highly compared to other insects. Our analyses lay the foundation for future comparative and experimental analyses that will establish *Heliconius* as a useful case study in evolutionary neurobiology.

INTRODUCTION

Behavioral adaptations are largely based in changes in brain function. In some cases this includes differential expansion of individual brain structures, or functionally related systems, that betray underlying changes in neuron number or circuitry. These provide an opportunity to study the neural basis of adaptive behavior, particularly in clades with known ecological specializations. The Neotropical genus *Heliconius* (Heliconiinae, Nymphalidae) display a number of striking behavioral adaptations including a dietary adaptation unique among Lepidoptera; adult pollen feeding (Gilbert, 1972, 1975). With the exception of four species formerly ascribed to the genus *Neruda* (Beltrán et al., 2007; Kozak et al., 2015), all *Heliconius* actively collect and ingest pollen as adults. This provides a source of amino acids and permits a greatly extended lifespan of up to six months without reproductive senescence (Gilbert, 1972; Benson, 1972; Ehrlich and Gilbert, 1973). Without access to pollen *Heliconius* suffer a major reduction in longevity and reproductive success (Gilbert, 1972; Dunlap-Pianka et al., 1977; O'Brien et al., 2003).

Several lines of evidence suggest selection for pollen feeding has shaped *Heliconius* foraging behavior. Pollen is collected from a restricted range of mostly Cucurbitaceous plants (Estrada and Jiggins, 2002), which occur at low densities (Gilbert, 1975). Individuals inhabit home ranges of typically less than 1 km^2, within which they repeatedly utilize a small number of roosting sites that they return to with high fidelity (Turner, 1971; Benson, 1972; Gilbert, 1975; Mallet, 1986; Murawski and Gilbert, 1986; Finkbeiner, 2014). On leaving the roost individuals visit feeding sites with a level of consistency in time and space that strongly suggests 'trap-lining' behavior (Ehrlich and Gilbert, 1973; Gilbert, 1975, 1993; Mallet, 1986), analogous to that observed in foraging bees (Janzen, 1971; Heinrich, 1979). Roosts themselves are located visually (Jones, 1930; Gilbert, 1972; Ehrlich and Gilbert, 1973; Mallet, 1986), and older individuals tend to be more efficient foragers (Boggs et al., 1981; Gilbert, 1993). Together these observations suggest the evolution of pollen feeding in *Heliconius* was facilitated by an enhanced, visually-orientated and time-compensated memory that utilizes long distance landmarks (Gilbert, 1975). The evolution of this behavior must involve "some elaboration of the nervous system" (Turner, 1981). This elaboration is suggested to occur in the mushroom bodies, which Sivinski (1989)

reported are 3–4 times larger in *Heliconius charithonia* than in six other species of butterfly, including two non-pollen feeding Heliconiini.

Insect mushroom bodies have a variety of roles in olfactory associative learning, sensory integration, filtering and attention (Zars, 2000; Farris, 2005, 2013; Menzel, 2014). Direct experimental evidence suggests the mushroom bodies mediate place memory in *Periplaneta americana* (Mizunami et al., 1998; Lent et al., 2007). Two lines of indirect evidence further implicate the mushroom bodies in allocentric memory in other insects. First, comparisons across species suggest that extreme evolutionary expansion of the mushroom body may commonly be associated with changes in foraging behavior that depend on spatial memory or the complexity of sensory information utilized by the species (Farris, 2005, 2013). For example, phylogenetic comparisons across Hymenoptera demonstrate the volumetric expansion and elaboration of the Euhymenopteran mushroom body occurs coincidently with the origin of parasitoidism (Farris and Schulmeister, 2011), a behavioral adaptation that involves place-centered foraging and spatial memory for host location (Rosenheim, 1987; van Nouhuys and Kaartinen, 2008). Second, mushroom bodies are ontogenetically plastic, and this plasticity has been linked to foraging behavior. Again, the trap-lining Hymenoptera illustrate the link between foraging behavior and the mushroom bodies (Withers et al., 1993; Durst et al., 1994; Capaldi et al., 1999; Farris et al., 2001). Honeybees show two forms of post-eclosion growth in mushroom body volume; age dependent growth, which occurs regardless of environmental variation, and experience dependent growth which increases with foraging or social experience (Withers et al., 1993; Durst et al., 1994; Fahrbach et al., 1998, 2003; Farris et al., 2001; Maleszka et al., 2009). In other Hymenoptera there is close correspondence between the rate and timing of mushroom body growth and the onset of foraging behavior (Gronenberg et al., 1996; Kühn-Bühlmann and Wehner, 2006; Withers et al., 2008; Jones et al., 2013). Whether the trap-lining behavior observed in *Heliconius* is associated with similar ontogenetic plasticity is not known.

Here we confirm Sivinksi's (1989) observation of a phylogenetic expansion of the mushroom bodies in *Heliconius*. We further demonstrate ontogenetic and environmentally induced plasticity comparable in size to trap-lining Hymenoptera. Together these analyses suggest the mushroom bodies may have a role in the allocentric spatial foraging observed in *Heliconius*, and lay the groundwork for

comparative analyses across Heliconiini examining the origin and timing of mushroom body expansion.

MATERIALS & METHODS

Animals

We collected five males and five females of two species of *Heliconius*, *H. hecale melicerta* and *H. erato demophoon* from wild populations around Gamboa (9°7.4′ N, 79°42.2′ W, elevation 60 m) and the nearby Soberanía National Park, República de Panamá. We assume all wild-caught individuals were sexually mature, and that the age range is not biased between species or sexes. Wild individuals were compared to individuals from first or second-generation insectary-reared stock populations, descended from wild caught parents from the same sampling localities. Stock populations were kept in controlled conditions in cages (c. 1 × 2 × 2 m) of mixed sex at roughly equal densities. Cages were housed at the *Heliconius* insectaries at the Smithsonian Tropical Research Institute's (STRI) facility in Gamboa. Stocks had access to their preferred host plant (*Passiflora biflora* and *P. vitifolia* respectively for *H. erato* and *H. hecale*), a pollen source (*Psychotria elata*) and feeders containing c. 20% sugar solution with an additional bee-pollen supplement to ensure an excess of pollen. Larvae were allowed to feed naturally on the host plant.

After emergence from the pupae insectary-reared individuals were collected for two age groups, a recently emerged 'young' group (1–3 days post emergence) and an 'old' group (2–3 weeks post emergence). *Heliconius* undergo a "callow" period of general inactivity immediately after emergence that lasts about 5 days, during which flight behavior is weak and males are sexually inactive (Mallet, 1980). These age groups therefore represent behaviorally immature and mature individuals. For *H. hecale* 5 males and 5 females were sampled for both age groups, in *H. erato* 4 males and 6 females were sampled for the 'young' group and 5 males and 4 females were sampled for the 'old' group. In samples for which the exact time of emergence was known there was no significant difference between *H. hecale* and *H. erato* in age structure of the old (*H. erato*: mean = 22.6 days, SD = 8.6; *H. hecale*: mean = 26.4 days, SD = 5.5; t_{13} = -0.899, p = 0.385) or young (*H. erato*: mean = 1.7 days, SD = 0.8; *H. hecale*: mean = 1.3 days, SD = 1.1; t_{17} = 0.829, p = 0.419) insectary-reared groups. Three body size measurements were taken for each individual: body mass,

166 weighted to 0.01 g using a OHAUS pocket balance (model YA102), body length, and
167 wingspan, measured using FreeLOGIX digital calipers. Samples were collected and
168 exported under permits SEX/A-3-12 and SE/A-7-13 obtained from the Autoridad
169 Nacional del Ambiente, República de Panamá in conjunction with STRI.
170
171 **Antibodies and sera for neuropil staining**
172 We used indirect immunofluorescence staining against synapsin to reveal the neuropil
173 structure of the brain under a confocal microscope (Ott, 2008). This technique
174 exploits the abundant expression of synapsin, a vesicle-associated protein, at
175 presynaptic sites. Monoclonal mouse anti-synapsin antibody 3C11 (anti-SYNORF1;
176 (Klagges et al., 1996) was obtained from the Developmental Studies Hybridoma Bank
177 (DSHB), University of Iowa, Department of Biological Sciences, Iowa City, IA
178 52242, USA (RRID: AB_2315424). The 3C11 antibody was raised against a
179 bacterially expressed fusion protein generated by adding a glutathione S-transferase
180 (GST)-tag to cDNA comprised of most of the 5′ open reading frame 1 of the
181 *Drosophila melanogaster* synapsin gene (*Syn,* CG3985). The binding specificity of
182 this antibody was characterised in *D. melanogaster* (Klagges et al., 1996) and
183 confirmed in synapsin null mutants by Godenschwege et al. (2004). The epitope was
184 later narrowed down to within LFGGMEVCGL in the C domain (Hofbauer et al.,
185 2009). Bioinformatic analysis has confirmed the presence of this motif in lepidopteran
186 genomes, and demonstrated that it is highly conserved across Lepidoptera
187 (Montgomery and Ott, 2015). Binding specificity in *M. sexta* has been confirmed by
188 western blot analysis (Utz et al., 2008) and 3C11 immunostaining has been used as an
189 anatomical marker of synaptic neuropil in a wide range of arthropod species including
190 several Lepidoptera: *D. plexippus* (Heinze and Reppert, 2012), *G. zavaleta*
191 (Montgomery and Ott, 2015), *H. virescens* (Kvello et al., 2009) and *M. sexta* (El
192 Jundi et al., 2009). Cy2-conjugated affinity-purified polyclonal goat anti-mouse IgG
193 (H+L) antibody (Jackson ImmunoResearch Laboratories, West Grove, PA) was
194 obtained from Stratech Scientific Ltd., Newmarket, Suffolk, UK (Jackson
195 ImmunoResearch Cat No. 115-225-146, RRID: AB_2307343).
196
197 **Immunocytochemistry**
198 Brains were fixed and stained following a published protocol (Ott, 2008). The
199 protocol was divided into two stages, the first of which was performed at the STRI

Gamboa Field Station. The brain was exposed under HEPES-buffered saline (HBS; 150 mM NaCl; 5 mM KCl; 5 mM $CaCl_2$; 25 mM sucrose; 10 mM HEPES; pH 7.4) and fixed in situ for 16–20 hours at room temperature (RT) in zinc-formaldehyde solution (ZnFA; 0.25% (18.4 mM) $ZnCl_2$; 0.788% (135 mM) NaCl; 1.2% (35 mM) sucrose; 1% formaldehyde) under agitation. The brain was subsequently dissected out under HBS, washed (3 × in HBS), placed into 80% methanol/20% DMSO for 2 hours under agitation, transferred to 100% methanol and stored at RT. After transportation to the UK samples were stored at -20˚C.

In the second stage of the protocol the samples were brought to RT and rehydrated in a decreasing methanol series (90%, 70%, 50%, 30%, 0% in 0.1 M Tris buffer, pH 7.4, 10 minutes each). Normal goat serum (NGS; New England BioLabs, Hitchin, Hertfordshire, UK) and antibodies were diluted in 0.1 M phosphate-buffered saline (PBS; pH 7.4) containing 1% DMSO and 0.005% NaN_3 (PBSd). After a pre-incubation in 5% NGS (PBSd-NGS) for 2 hours at RT, antibody 3C11 was applied at a 1:30 dilution in PBSd-NGS for 3.5 days at 4˚C under agitation. The brains were rinsed in PBSd (3 × 2 hours) before applying the Cy2-conjugated anti-mouse antibody 1:100 in PBSd-NGS for 2.5 days at 4˚C under agitation. This was followed by increasing concentrations of glycerol (1%, 2%, 4% for 2 hours each, 8%, 15%, 30%, 50%, 60%, 70% and 80% for 1 hour each) in 0.1 M Tris buffer with DMSO to 1%. The brains were then passed in a drop of 80% glycerol directly into 100% ethanol. After agitation for 30 minutes the ethanol was refreshed (3 × 30 minute incubations), before being underlain with methyl salicylate. The brain was allowed to sink, before the methyl salicylate was refreshed (2 × 30 minute incubations).

Confocal imaging

All imaging was performed on a confocal laser-scanning microscope (Leica TCS SP8, Leica Microsystem, Mannheim, Germany) using a 10× dry objective with a numerical aperture of 0.4 (Leica Material No. 11506511), a mechanical *z*-step of 2 µm and an *x*-*y* resolution of 512 × 512 pixels. Imaging the whole brain required capturing 3×2 tiled stacks in the *x*-*y* dimensions (20% overlap) that were automatically merged in Leica Applications Suite Advanced Fluorescence software. Each brain was scanned from the posterior and anterior side to span the full *z*-dimension of the brain. These image stacks were then merged in Amira 3D analysis software 5.5 (FEI Visualization

Sciences Group; custom module 'Advanced Merge'). The *z*-dimension was scaled 1.52× to correct the artifactual shortening associated with the 10× air objective (Heinze and Reppert, 2012; Montgomery and Ott, 2015). Images that illustrate key morphological details were captured separately as single confocal sections with an *x*-*y* resolution of 1024 × 1024 pixels.

Neuropil segmentations and volumetric reconstructions

We assigned image regions to anatomical structures in the Amira 5.5 *labelfield* module by defining outlines based on the brightness of the synapsin immunofluorescence. Within each stack, every forth or fifth image was manually segmented and interpolated in the *z*-dimension across all images that contain the neuropil of interest. The *measure statistics* module was used to determine volumes (in μm^3) for each neuropil. 3D polygonal surface models of the neuropils were constructed from the smoothed labelfield outlines (*SurfaceGen* module). The color code used for the neuropils in the 3D models is consistent with previous neuroanatomical studies of insect brains (Brandt et al., 2005; Kurylas et al., 2008; El Jundi et al., 2009a, b; Dreyer et al., 2010; Heinze and Reppert, 2012; Montgomery and Ott, 2015).

The whole-brain composite stacks were used to reconstruct and measure six paired neuropils in the optic lobes, and seven paired and two unpaired neuropils in the midbrain where distinct margins in staining intensity delineate their margins. All paired neuropils were measured on both sides of the brain in wild-caught individuals to permit tests of asymmetry, yielding two paired measurements per brain (*i.e.* $N = 10 \times 2$) for each structure. We found no evidence of volumetric asymmetry for either species ($p > 0.05$ for each neuropil in a paired t-tests) and therefore summed the volumes of paired neuropil to calculate the total volume of that structure. In insectary-reared individuals we subsequently measured the volume of paired neuropil from one hemisphere, chosen at random, and multiplied the measured volume by two. We measured the total neuropil volume of the midbrain to permit statistical analyses that control for allometric scaling. In keeping with the earlier lepidopteran literature, we use the term 'midbrain' for the fused central mass that comprises the protocerebral neuromere excluding the optic lobes, the deuto- and tritocerebral neuromeres, and the sub-esophageal neuromeres. For the following statistical analyses we analyzed the

266 central body as a single structure and, unless otherwise stated, summed the volumes
267 of the mushroom body lobes and peduncles.
268
269 **Intraspecific statistical analyses**
270 In all statistical analyses continuous variables were $\log_{10}$-transformed. Unpaired two-
271 tailed two-sample *t*-tests were used to test for volumetric differences between sexes or
272 groups. We found no evidence of sexual dimorphism in neuropil volume of wild
273 caught individuals that could not be explained by allometric scaling and therefore
274 combined male and female data.
275 All statistical analyses were performed in R v.3.1 (R Development Core
276 Team, 2008). Our analyses focused on two intra-specific comparisons: i) we
277 compared 'young' and 'old' insectary-reared individuals and interpret significant
278 differences as evidence for post-eclosion growth; and ii) we compared wild-caught
279 individuals with 'old' insectary-reared individuals and interpret significant differences
280 as evidence for environmentally induced, or experience dependent plasticity. These
281 comparisons were made by estimating the allometric relationship between each
282 neuropil and a measure of overall brain size (total volume of the midbrain minus the
283 combined volume of all segmented neuropil in the midbrain: 'rest of midbrain', rMid)
284 using the standard allometric scaling relationship: $\log y = \beta \log x + \alpha$. We used
285 standard major axis regressions in the SMATR v.3.4-3 (Warton et al., 2012) to test for
286 significant shifts in the allometric slope (β). Where we identified no heterogeneity in
287 β we performed two further tests: 1) for differences in α that suggest discrete 'grade-
288 shifts' in the relationship between two variables, 2) for major axis-shifts along a
289 common slope. Patterns of brain:body allometry were explored in a similar manner,
290 using total neuropil volume as the dependent variable (summed volumes of all optic
291 lobes neuropil plus the total midbrain volume), and comparing the results obtained
292 using alternative body size measurements as the independent variable. We also
293 present the effect size, measured by the correlation coefficient (*r*). Effect sizes of
294 $0.1<r<0.3$ are interpreted as 'small' effects, $0.3<r<0.5$ 'medium' effects, and $r<0.5$
295 'large' effects (Cohen, 1988).
296
297 **Interspecific statistical analyses**
298 To analyze interspecific patterns of divergence in brain composition we collected
299 published data for neuropil volumes of four other Lepidoptera; *D. plexippus*; (Heinze

and Reppert, 2012), *G. zavaleta* (Montgomery and Ott, 2015), *M. sexta*; (El Jundi et al., 2009a) and *H. virescens* (Kvello et al., 2009). Data were available for eight neuropils across all four species. Relative size was measured by calculating the residuals from a phylogenetically-corrected least squares (PGLS) linear regression between each structure and the rest of the brain (whole brain or midbrain as indicated) performed in BayesTraits (freely available from www.evolution.rdg.ac.uk; Pagel, 1999). For this analysis, a phylogeny of the six species was created using data on two loci, *COI* and *EF1a* (GenBank Accession IDs, *COI*: EU069042.1, GU365908.1, JQ569251.1, JN798958.1, JQ539220.1, HM416492.1; *EF1a*: EU069147.1, DQ157894.1, U20135.1, KC893204.1, AY748017.1, AY748000.1). The data were aligned and concatenated using MUSCLE (Edgar, 2004), before constructing a maximum likelihood tree in MEGA v.5 (Tamura et al., 2011). Differences in brain composition across species were analyzed by Principal Component analysis of these data, and visualized as biplots (Greenacre, 2010) in R package *ggbiplot* (V.Q. Vu, https://github.com/vqv/ggbiplot). Finally, we extended our phylogenetic analysis across insects using a similar approach. We restricted this analysis to volumetric data collected with similar methodology (Rein et al., 2002; Brandt et al., 2005; Kurylas et al., 2008; Dreyer et al., 2010; Ott and Rogers, 2010; Wei et al., 2010). The phylogenetic relationship of these insects was taken from Trautwein et al. (2012).

RESULTS

General layout of the *Heliconius* brain

The overall layout and morphology of the *Heliconius* brain (Fig. 1) is similar to that of other Lepidoptera (El Jundi et al., 2009; Kvello et al., 2009; Heinze and Reppert, 2012a; Montgomery and Ott, 2015). The midbrain forms a single medial mass, containing the supra-esophageal ganglion to which the sub-esophageal ganglion is fused. Together with the rest of the midbrain (rMid), which lacks distinct internal boundaries and was therefore unsuitable for further segmentation in the current analysis, we measured the volumes of six paired neuropils in the optic lobes, and eight paired and two unpaired neuropils in the midbrain in 59 individuals across both species (Table 1).

Sensory neuropil

The large optic lobes (OL; Fig. 2) account for approximately 64% of the total brain volume. As is the case in both *D. plexippus* and *G. zavaleta* the lamina (La), two-layered medulla (Me) (Fig. 2E), accessory medulla (aMe), lobula (Lob) and lobula plate (Lop) are well defined and positioned in the OL as nested structures from lateral to medial (Fig. 2A). The La has a distinct, brightly stained inner rim (iRim; Fig. 2E), a feature common to all diurnal butterflies analyzed thus far (Heinze and Reppert, 2012; Montgomery and Ott, 2015). In common with *D. plexippus* we identify a thin strip of irregularly shaped neuropil running ventrally from the aME to the Me (Fig. 2G–H).

We also identify a sixth neuropil in the OL that we believe to be homologous to the optic glomerulus (OG; Fig. 2B,F) identified in *D. plexippus* (Heinze and Reppert, 2012), which is absent in other lepidopteran brains described to date and was postulated to be Monarch-specific. As in *D. plexippus* this neuropil is a multi-lobed, irregularly shaped structure positioned to the medial margin of the Lob with which it appears to be connected. In *Heliconius* the OG is not as extended in the anterior margin as in *D. plexippus* and is subsequently confined to the OL, without protrusion into the optic stalk or midbrain (Fig. 2A,B,F). The position of the OG in *Heliconius* is also similar to that of a much smaller neuropil observed in *G. zavaleta* (Montgomery and Ott, 2015) that may be homologous.

The midbrain contains further neuropils with primary functions in processing visual information that include the anterior optic tubercule (AOTu). We identify the same four components of the AOTu previously described in *D. plexippus* and *G. zavaleta* butterflies (Heinze and Reppert, 2012; Montgomery and Ott, 2015): the small, closely clustered nodular unit (NU), strap (SP) and lower unit (LU), and the much larger upper unit (UU) (Fig. 2C). As in other butterflies, the UU is expanded compared with nocturnal moths (El Jundi et al., 2009; Kvello et al., 2009). The proportion of total neuropil comprised of the AOTu is, however, larger in *D. plexippus* (0.74%) than *Heliconius* (0.40% in *H. hecale* and 0.37% in *H. erato*).

The antennal lobes (AL), the primary olfactory neuropil, are comprised of small, round glomeruli that are innervated by axons from olfactory receptor neurons in the antennae. These glomeruli are arranged around a Central Fibrous Neuropil (CFN) (Figure 3A,B). In *Heliconius* the AL comprises 2% of the total brain neuropil volume, and contains approximately 68 glomeruli (estimated in one individual of each sex: *H. erato* ♂ = 69, ♀ = 68; *H. hecale* ♂ = 68, ♀ = 67) which matches closely the number of olfactory receptor genes (70) identified in the *H. melpomene* genome

(Dasmahapatra et al., 2012). We found no expanded macro-glomeruli complex (MGC) or obvious candidates for sexually dimorphic glomeruli. This is in keeping with all diurnal butterflies described to date (Rospars, 1983; Heinze and Reppert, 2012; Carlsson et al., 2013), with the exception of the more olfactorily orientated *G. zavaleta* (Montgomery and Ott, 2015).

We took advantage of comparable datasets for *H. erato, H. hecale* and *G. zavaleta* to investigate whether changes in relative AL volume are due to an increased volume of glomeruli or CFN. Both glomerular and CFN volume are larger in *G. zavaleta* relative to midbrain volume, as indicated by significant grade-shifts in allometric scaling in *G. zavaleta* and *Heliconius* (glomerular, *H. erato*: Wald $\chi2 = 10.709$, $p = 0.001$; *H. hecale*: Wald $\chi2 = 9.139$, $p = 0.003$; CFN, *H. erato*: Wald $\chi2 = 30.282$, $p < 0.001$; *H. hecale*: Wald $\chi2 = 26.638$, $p < 0.001$). However, CFN expansion in *G. zavaleta* is disproportionately large, driving a grade-shift in the scaling relationship between glomerular and CFN volume in *G. zavaleta* when compared with either *Heliconius* (*H. erato*: Wald $\chi2 = 19.680$, $p < 0.001$; *H. hecale*: Wald $\chi2 = 31.663$, $p < 0.001$; Fig. 3D).

Central complex

The central complex is a multimodal integration center linked to a range of functions from locomotor control to memory (Pfeiffer and Homberg, 2014). Within the limitations of the current analysis, the anatomy of the *Heliconius* central complex shows strong conservation with *D. plexippus* and *G. zavaleta* (Heinze and Reppert, 2012; Montgomery and Ott, 2015). The central body (CB) is positioned along the midline of the central brain and is formed of two neuropils, the upper (CBU) and lower (CBL) divisions, which are associated with small paired neuropils, the noduli (No), located ventrally to the CB (Fig. 4A–D,G). Two further paired neuropils, the protocerebral bridge (PB; Fig. 4A,E) and posterior optic tubercles (POTu; Fig. 4A,F), are positioned towards the posterior margin of the brain.

Mushroom bodies

The most striking aspect of *Heliconius* brain morphology is the hugely expanded mushroom bodies which span the depth of the brain along the anterior-posterior axis (Fig. 5). On the anterior side, the mushroom body lobes (MB-lo) lie above the AL. As in *D. plexippus* (Heinze and Reppert, 2012) the distinct lobe structure observed in

401 moths (El Jundi et al., 2009; Kvello et al., 2009) is lost, possibly due to extensive
402 expansion. The only identifiable feature is a lobe curving round the medial margin,
403 likely to be part of the vertical lobe (Fig. 5D,F). The MB-lo merges with the
404 cylindrical pedunculus (MB-pe) that extends to the posterior midbrain. The boundary
405 between the MB-lo and MB-pe is not distinct. The combined volume of the MBlo+pe
406 accounts for 12.2% of total midbrain volume in *H. hecale* and 14.6% of total midbrain
407 volume in *H. erato*, at least twice that reported for other Lepidoptera (Sjöholm et al.,
408 2005; El Jundi et al., 2009; Kvello et al., 2009; Heinze and Reppert, 2012a;
409 Montgomery and Ott, 2015). At the posterior end, the MB-pe splits into two roots that
410 are encircled by the mushroom body calyx (MB-ca; Fig. 5A,H,K). A Y-tract runs
411 parallel to the MB-pe from the posterior boundary of the MB-lo to the junction
412 between the MB-pe and MB-ca. The Y-tract ventral loblets seen in other Lepidoptera
413 (El Jundi et al., 2009; Kvello et al., 2009) are not distinct, having merged with the
414 MB-lo (Fig. 5A,J,N).

415 *Heliconius* have an un-fused double MB-ca with a deeply cupped morphology
416 (Fig. 5A,C). Two concentric zones can be identified (Fig. 5E), though the boundary is
417 not distinct throughout the depth of the neuropil. The MB-ca comprises 20.7% and
418 23.9% of total midbrain volume in *H. hecale* and *H. erato* respectively, at least three
419 times greater than reported in other Lepidoptera (Sjöholm et al., 2005; El Jundi et al.,
420 2009; Kvello et al., 2009; Heinze and Reppert, 2012a; Montgomery and Ott, 2015). In
421 some individuals the MB-ca is so large that it protrudes into the OL resulting in a
422 distortion of shape caused by constriction around the optic stalk (Fig. 5H). We also
423 observe some degree of pitting in the posterior surface of the MB-ca (Fig. 5I). This
424 pitting is related to radially arranged columnar domains that are apparent within the
425 calycal neuropil (Fig. 5J,K). We do not observe any structure clearly identifiable as an
426 accessory calyx. We do see a brightly stained globular neuropil below the MB-ca/pe
427 junction but it is quite some distance away from the junction and lacks the 'spotty'
428 appearance of the accessory calyx in *D. plexippus* (Heinze and Reppert, 2012). It
429 seems more likely that this structure is a 'satellite' neuropil that is not part of the MB
430 (Farris, 2005). Its position corresponds roughly to the medial end of the expanded OG
431 in *D. plexippus*. In some preparations one can follow a narrow faint fiber tract from
432 here to an area of more intense staining in the optic stalk and on to the medial margin
433 of the OG. If this is a functional connection, it is conceivable that the medial
434 expansion of the OG in *D. plexippus* occurred along this pre-existing pathway.

435

436 **Interspecific divergence in brain composition and mushroom body expansion in**
437 ***Heliconius***

438 After correcting for allometric scaling by phylogenetically-corrected regressions
439 against total neuropil volume, the six lepidopteran species can be separated along the
440 first two principal components that together explain 90.7% of variance. PC1 (65.9%
441 of Var) is heavily loaded by sensory neuropil in one direction, and the MB-ca and
442 MB-lo+ped in the other (Table 2). PC2 (24.8% of Var) is heavily loaded by the Me in
443 one direction and the AL and CB in the other. This roughly separates the six species
444 into three pairs, representing (i) *H. hecale* and *H. erato*; (ii) the other diurnal
445 butterflies, *D. plexippus* and *G. zavaleta*; and (iii) the night-flying moths, *H. virescens*
446 and *M. sexta* (Fig. 6B). When midbrain neuropil are analyzed separately, PC1 (68.7%
447 of Var) marks an axis dominated by AL, CB and MB, and PC2 (23.3% of Var) is
448 strongly loaded by the AOTu (Fig. 6C). This leads to two clusters grouping (i) *H.*
449 *hecale* and *H. erato*, which invest heavily in the mushroom body neuropil, and (ii) the
450 night-flying moths and *G. zavaleta*, which invest heavily in olfactory neuropil;
451 leaving *D. plexippus* isolated by its large AOTu volume.

452 The combined volume of the calyx, pedunculus and lobes account for 13.7%
453 of total brain neuropil volume in *H. erato*, and 11.9% in *H. hecale*. This is much
454 larger than reported for any other Lepidoptera measured with similar methods (range
455 2.3–5.1%). Expressed as a percentage of the midbrain, to remove the effects of
456 variation in the large OL, *H. erato* (38.5%) and *H. hecale* (32.9%) again exceed other
457 Lepidoptera (4.8–13.5%) by 3–7 fold. These figures are also much larger than
458 reported for *H. charithonia* (4.2% of total brain size) by Sivinski (1989), whose
459 figures for other Lepidoptera are also much lower suggesting the difference is
460 explained by variation in methodology.

461 Beyond Lepidoptera, the most comparable data available are from *Apis*
462 *mellifera* (Brandt et al., 2005) and *Schistocerca gregaria* (Kurylas et al., 2008) for
463 which mushroom body volume and midbrain volume are reported (Fig. 6D). In terms
464 of raw volume (Table 1) *Heliconius* mushroom bodies are roughly equal in size to *A.*
465 *mellifera*. However, in *A. mellifera* the mushroom bodies comprise 65.4% of the
466 midbrain, (40.6% MB-ca, 24.8% MB-lo+ped) (Brandt et al., 2005), in gregarious-
467 phase *S. gregaria* they comprise 15.1% (8.2% MB-ca including the accessory calyx,
468 6.3% MB-lo+ped) (Kurylas et al., 2008). Further comparisons can be made

469 expressing mushroom body size as a percentage of segmented neuropil (Me+Lobula
470 system, CB, MB and AL) that were labeled across a wider range species. As a ratio of
471 percentage mushroom body volume to the percentage of the two other midbrain
472 neuropil (AL and CB), *Heliconius* have ratios (*H. erato*: 6.4; *H. hecale*: 6.7) that
473 exceed even *A. mellifera* (3.8). To account of the dominant effect of OL size on
474 scaling with overall brain size we also analysed residual variance from a PGLS
475 regression (Fig. 6E) between percentage OL and percentage MB volume. This shows
476 *Heliconius* (*H. erato* +8.2; *H. hecale* +7.5) have the second largest residual MB size
477 following *A. mellifera* (+11.9).
478
479 **Brain : body allometry**
480 In both species, larger wild individuals have larger brains when using total neuropil
481 volume and either body length or wingspan as measures of brain and body size (log-
482 log SMA regression, *H. hecale,* body length $p = 0.020$; wingspan $p = 0.019$; *H. erato,*
483 body length $p = 0.011$; wingspan $p = 0.010$). The brain size : body *mass* relationship
484 is not significant in wild individuals (*H. hecale,* $p = 0.055$; *H. erato,* $p = 0.863$), most
485 likely because body mass varies much with reproductive state and feeding condition.
486 We therefore used body length as a proxy for body size to analyze the effect of age
487 and experience on the relative size of the brain.
488 Both species showed a clear grade-shift with age towards increased relative
489 brain size (*H. hecale:* Wald $\chi^2 = 5.780$, $p = 0.016$; *H. erato:* Wald $\chi^2 = 10.124$, $p =$
490 0.001). Body length was very similar in old and young individuals (*H. hecale* $t_{18} = -$
491 0.918, $p = 0.371$; *H. erato* $t_{17} = 0.581$, $p = 0.568$) suggesting the effect reflects an
492 increase in absolute neuropil volume. Indeed, old individuals had significantly larger
493 absolute midbrain volumes in both species (*H. erato:* $t_{17} = 4.192$, $p = 0.001$, $r = 0.713$;
494 *H. hecale:* $t_{18} = 3.054$, $p = 0.007$, $r = 0.595$; Fig. 7A,D). An absolute increase in OL
495 and total brain volume, however, was strongly supported only in *H. erato* (OL: $t_{17} =$
496 5.076, $p < 0.001$, $r = 0.776$; total, $t_{17} = 5.153$, $p < 0.001$, $r = 0.708$) and not evident in
497 *H. hecale* (OL, $t_{18} = 0.280$, $p = 0.783$; total, $t_{18} = 1.082$, $p = 0.293$).
498 Only *H. hecale* showed a clear response in overall brain size to experience.
499 The total neuropil was 40% larger in wild-caught than in old insectary-reared
500 individuals ($t_{17} = 2.553$, $p = 0.020$, $r = 0.526$) driven by a significant difference in
501 midbrain volume ($t_{17} = 3.658$, $p = 0.002$, $r = 0.664$), but not OL volume ($t_{18} = 1.728$, p
502 $= 0.101$; Fig. 7D). Although there was no matching difference in body length ($t_{18} =$

503 0.983, p = 0.436), a grade-shift towards larger relative brain size in wild *hecale* was
504 not supported (Wald χ^2 = 2.058, p = 0.151). However, we do observe a grade-shift
505 when the midbrain is analyzed separately (Wald χ^2 = 4.725, p = 0.030). No significant
506 brain or body size differences were found between wild and old insectary-reared
507 individuals in *H. erato* (total neuropil: t_{17} = -0.432, p = 0.671; midbrain: t_{17} = -0.732, p
508 =0.474; OL: t_{17} = -0.123, p = 0.904; body length: t_{17} = 1.009, p = 0.327; Fig. 7A).
509
510 **Post-eclosion growth in the volume of individual neuropil regions**
511 The age-related increase in overall absolute brain size in *H. erato* was reflected in
512 volumetric increases in nearly all brain regions, with only the OG failing to show a
513 significant expansion in old individuals (Table 3A). There was some evidence for
514 age-related differences in the allometric scaling coefficients for aMe and PB, and for
515 grade-shifts in OG and POTu, but these were weak relative to the strong major axis
516 shifts observed for all neuropils investigated (Table 3A). The largest shifts were
517 observed for the POTu (difference in fitted-axis mean, Δ_{FA} = 0.604), aME (Δ_{FA} =
518 0.536), MB-ca (Δ_{FA} = 0.496) and MB-lo+ped (Δ_{FA} = 0.393; Fig. 8A-C).
519 In contrast, in *H. hecale,* age-related size increases in volume were confined to
520 the midbrain and not all segmented midbrain regions showed the same pattern of
521 expansion; the rMid, components of the mushroom body complex, central complex
522 and AL were all significantly larger in old individuals, but the AOTu, POTu and all
523 optic lobe neuropil were not (Table 3B). Neuropil expansion appears to occur in a co-
524 ordinated manner, such that the allometric relationship between each neuropil and
525 rMid is maintained (Table 3B). The only exceptions were the La, Me and OG, which
526 showed significant grade-shifts towards a reduced volume relative to rMid in old
527 individuals. All other segmented neuropil showed major-axis shifts along a common
528 slope towards higher values in old individuals (Table 3B). The largest shifts were
529 observed in the mushroom body (MB-ca, Δ_{FA} = 0.279; MB-lo+ped, Δ_{FA} = 0.250;
530 Fig. 8A1–C1).
531
532 **Experience-dependent plasticity in neuropil volume**
533 Although wild *H. erato* do not have significantly larger absolute volumes for any
534 measured neuropil (Table 4A), differences in allometric scaling or grade-shifts
535 between wild and old insectary-reared individuals are nevertheless evident. Altered
536 scaling affects the MB-ca, Lop, and PB, all of which show shallower scaling

relationships (smaller β) with rMid in wild-caught individuals (Table 4A; Figure 7B,C). The MB-lo+ped shows an unambiguous grade-shift towards larger size in wild whilst maintaining a common slope, and also shows a major axis shift (Δ_{FA} = 0.250; Fig. 8B1).

In *H. hecale* wild individuals have significantly larger total midbrains (t_{18} = 3.658, p = 0.002). The only segmented neuropil to reflect this difference, however, are the MB-ca and MB-lo+ped (Table 4B; Fig. 8A2,C2), while the rMid is also larger in wild individuals (t_{18} = 3.417, p = 0.003). The average MB-ca volume of old insectary-reared individuals is only 68.3% of the average wild MB-ca volume, for the young insectary-reared individuals it is 49.3% (Figure 8A2,C2). For MB-lo+pe these figures are 76.9% and 58.7% respectively (Figure 8A2,B2). For comparison, in *H. erato* the average MB-ca volume of old insectary-reared individuals is 96.2% of the average wild MB-ca volume, for the young insectary-reared individuals it is 59.7% (Fig. 8A1–C1). For MB-lo+pe these figures are 96.9% and 63.9% respectively (Fig. 8A1–C1).

The only neuropil in the optic lobes to differ significantly in volume in *H. hecale* is the Me. The allometric relationship between neuropil volumes and rMid differs for all neuropil either in the allometric scaling coefficient or the intercept, except for the mushroom body components and aMe (Table 4A; Figure 7E,F). However, for aME this pattern is caused by a lack of allometric scaling in insectary-reared individuals (SMA p = 0.552). The mushroom bodies show evidence of a major axis shift along a common slope (MB-ca, Δ_{FA} = 0.355; MB-lo+ped, Δ_{FA} = 0.299; Fig 8B2, C2). Given all grade-shifts result in smaller neuropil volumes relative to rMid volume (Fig. 7E,F) we interpret this as indicating the rMid and mushroom bodies show coordinated environment-dependent increases in volume whilst other neuropil volumes remain largely constant, but with subsequently altered allometric relationships with rMid.

Allometric scaling of mushroom body components

We further explored the allometric scaling relationships between the three main mushroom body components, the MB-lo and MB-pe (analyzed separately), and the MB-ca. Within wild caught individuals, pairwise comparisons between these structures do not reveal any significant deviation from isometric scaling relationships (test $\beta \neq 1$, $p > 0.05$). However, the ontogenetic growth we observe between the

young and old groups of both species occur through concerted expansion of the MBlo and MBca (i.e. a major axis shift), both of which show grade-shifts in their allometric scaling with the MBpe between the young and old groups (Table 5A). A similar pattern is found comparing *H. hecale* wild and old groups, but there are no significant differences between wild and old *H. erato* with the exception of a narrowly significant difference in the scaling coefficient suggesting MB-lo becomes disproportionally larger as MB-ca increases in wild individuals compared to insectary reared individuals (Table 5B).

DISCUSSION

We have described the layout and volume of the major brain neuropils in two species of *Heliconius* butterflies. Our analyses illustrate the role ecology plays in shaping brain structure, and confirm the substantial evolutionary expansion of the *Heliconius* mushroom body first noted by Sivinski (1989). Indeed, our data suggest this previous work underestimated their size. We have further identified neuropil-specific patterns of volumetric variation across young and old insectary-reared and wild individuals that indicate significant post-eclosion growth and experience-dependent plasticity. In the mushroom body, the timing and extent of this ontogenetic plasticity is comparable to that found in insects that strongly rely on spatial memory for foraging (e.g. Withers et al., 1993, 2008; Gronenberg et al., 1996; Fahrbach et al., 1998, 2003; Maleszka et al., 2009; Jones et al., 2013).

Interspecific divergence and mushroom body expansion in Heliconius

Our interspecific analyses across Lepidoptera reveal an unambiguously mosaic pattern of brain evolution (Barton and Harvey, 2000), where the size of individual neuropils deviate from the allometric expectation. Mosaic patterns in mammals, fishes and ants have been interpreted as strong evidence for evolutionary responses to a species' particular ecological needs (Barton et al., 1995; Huber et al., 1997; Gronenberg and Hölldobler, 1999). In Lepidoptera, this is particularly noticeable in the sensory neuropils (Fig. 6B). The relative volume of the visual neuropils closely reflects diel activity patterns, and the size of the antennal lobes also appears to be strongly associated with a nocturnal or low-light diurnal niche. This is illustrated in a PCA of midbrain neuropil (Fig. 6C) that clusters the olfactorily driven butterfly *G.*

603 *zavaleta* with night-flying moths (Montgomery and Ott, 2015). Our data further
604 indicate that much of the divergence in AL size among Lepidoptera reflects changes
605 in CFN volume rather than total glomerular volume, implying that changes in the
606 number or branching complexity of AL interneurons dominate over numerical
607 differences in afferent sensory neuron supply, and associated sensitivity. Similarly,
608 the relative constancy in AL glomeruli number indicates that the dimensionality of the
609 afferent coding space is comparable across Lepidoptera with divergent diel patterns
610 (Boeckh and Boeckh, 1979; Rospars, 1983; Berg et al., 2002; Huetteroth and
611 Schachtner, 2005; Masante-Roca et al., 2005; Skiri et al., 2005; Kazawa et al., 2009;
612 Heinze and Reppert, 2012; Carlsson et al., 2013; Montgomery and Ott, 2015).
613 In contrast with other species-differences that are dominated by changes in the
614 sensory neuropils, *Heliconius* are clearly set apart in our multivariate analysis along
615 an axis heavily loaded by the mushroom bodies. As a percentage of total brain
616 volume, or indeed as a raw volume, *Heliconius* have the largest mushroom body so
617 far reported in Lepidoptera (Sivinski, 1989; Sjöholm et al., 2005; Rø et al., 2007;
618 Kvello et al., 2009; Snell-Rood et al., 2009; Dreyer et al., 2010; Heinze and Reppert,
619 2012b; Montgomery and Ott, 2015) and one of the largest across insects. This
620 phylogenetic expansion must reflect adaptive change in mushroom body function in
621 response to ecological selection pressures. The derived pollen-feeding behavior of
622 *Heliconius* provides a likely source of this selection (Sivinski, 1989). Several studies
623 have reported this behavior to entail spatially and temporally faithful foraging
624 patterns, guided by visual landmarks (Ehrlich and Gilbert, 1973; Gilbert, 1975, 1993;
625 Mallet, 1986) comparable with the landmark-based trap-lining behavior of foraging
626 bees. Experimental interventions (Mizunami et al., 1998) and comparative neuro-
627 ecological studies (Farris and Schulmeister, 2011) implicate mushroom bodies in
628 visually based spatial memory.
629 Comparisons across *Heliconius* and non-pollen feeding Heliconiini may
630 provide a test of this spatial memory hypothesis. Sivinski (1989) reported that two
631 individuals of *Dione juno* and *Dryas iulia*, both non-pollen feeding allies to
632 *Heliconius*, had mushroom bodies within the size range of other Lepidoptera. This
633 provides preliminary support that mushroom body expansion coincided with a single
634 origin of pollen feeding at the base of *Heliconius*. However, sampling in a wider
635 range of genera, including the specious *Eueides* which is most closely related to

636 *Heliconius* (Beltrán et al., 2007; Kozak et al., 2015), is required to confirm this
637 conclusion.

638 Alternative selection pressures also need to be considered, including the
639 degree of host-plant specialization (Brown, 1981) and the evolution of social roosting
640 (Benson, 1972; Mallet, 1986). These factors may well be inter-related, as visits to
641 *Passiflora* may be incorporated into trap-lines between pollen plants (Gilbert, 1975,
642 1993), and the sedentary home-range behavior required for trap-lining may predispose
643 *Heliconius* to sociality (Mallet, 1986). The latter scenario would parallel the
644 hypothesized origin of sociality in hymenoptera and primates in exaptations of an
645 expanded brain that may have first evolved to support specialization in foraging
646 behavior (Barton, 1998; Farris and Schulmeister, 2011). Regardless of whether pollen
647 feeding provided the initial selection pressure for mushroom body expansion, it is
648 likely that it contributes to meeting the energetic costs of increased neural investment.
649

650 ***Age- and experience-dependent growth in neuropil volume***

651 In both *H. erato and H. hecale*, the mushroom bodies are significantly larger in aged
652 individuals. Volume increases of 38.0% for the calyx and 34.0% for the lobe system
653 in *H. erato,* and 27.9% for the calyx and 23.7% for the lobes in *H. hecale* are
654 comparable to, if not greater than, the ontogenetic changes seen in Hymenoptera (e.g.
655 c. 30% in *Camponotus floridanus* (Gronenberg et al., 1996); c. 20% in *Bombus*
656 *impatiens* (Jones et al., 2013)). Our comparisons between aged insectary-reared and
657 wild caught individuals also identify experience-dependent plasticity. This
658 'experience' in the wild likely includes greater range of movement, greater challenges
659 in foraging, and more variable environmental conditions and social interactions.

660 Our data suggest experience-dependent plasticity particularly affects
661 mushroom body maturation, though the pattern differs between species. In *H. hecale* a
662 strong volumetric difference is found between old insectary-reared and wild caught
663 individuals for both the calyx (32%) and lobes (24%). A concomitant expansion of
664 the unsegmented midbrain results in a pronounced major-axis shift. This is not simply
665 the result of an increased total brain size, however: no other neuropil region shows a
666 comparable increase in wild caught individuals, resulting in widespread grade-shifts
667 in these other neuropils towards smaller size relative to the unsegmented midbrain.
668 This may reflect a coordinated growth between the mushroom bodies and
669 unsegmented midbrain areas or, alternatively, coincident independent expansions. In

H. erato old insectary-reared and wild-caught individuals have mushroom bodies of similar absolute size, but allometric grade-shifts over the unsegmented midbrain result in greater relative volumes in wild compared to insectary-reared individuals. The cause of this species difference is unclear, but warrants further investigation.

Finally, it is also notable that plasticity, in particularly age-related growth, is not restricted to the mushroom bodies. Several visual and olfactory neuropils show age- and experience-dependent expansions in *Heliconius,* as they do in other insects (Kühn-Bühlmann and Wehner, 2006; Snell-Rood et al., 2009; Ott and Rogers, 2010; Smith et al., 2010; Heinze and Florman, 2013; Jones et al., 2013). We also find evidence of plasticity in components of the central complex. In *D. plexippus*, size plasticity in the central body and protocerebral bridge has been linked to migratory experience and, by association, the sky compass navigation that supports it (Heinze et al., 2013). The occurrence of similar plasticity in non-migratory butterfly species implies that it may be associated with foraging or locomotor experience more generally, even at much smaller spatial scales.

Functional relevance of phylogenetic mushroom body expansion

Phylogenetic trends towards larger mushroom bodies involve increases in Kenyon Cell (KC) numbers, clustered into larger numbers of functional sub-units (Farris, 2008). Farris and Roberts (2005) suggest that increasing KC number may provide greater computational capacity by facilitating the processing of more complex combinatorial inputs from afferent projection neurons (Sivan and Kopell, 2004), or through integration across increasingly specialized sub-units (Strausfeld, 2002).

Novel pathways between such specialized KC sub-populations may play an important role in the origin of derived behaviors that require the integration of different sensory modalities (Chittka and Niven, 2009; Strausfeld et al., 2009). Examples of this are provided by Hymenoptera and phytophagous scarab beetles where, in addition to olfactory inputs, the mushroom body calyx receives direct input from the optic lobes (Gronenberg, 2001; Farris and Roberts, 2005; Farris and Schulmeister, 2011). This additional input is reflected in the subdivision of the calyx into the lip, which processes olfactory information, and the collar and basal ring, which process visual information (Gronenberg and Hölldobler, 1999). Visual input to the mushroom bodies has also been demonstrated in some butterflies (Snell-Rood et al., 2009) and moths (Sjöholm et al., 2005) but it has yet to be investigated in

Heliconius. The *Heliconius* calyx lacks the clear zonation observed in *D. plexippus* that has been suggested to be analogous to the *A. mellifera* lip, collar and basal ring (Heinze and Reppert, 2012). We do not interpret the lack of distinct zonation in *Heliconius* as evidence against functional sub-division, as *Spodoptera littoralis* displays localization of visual processing in the calyx that is not apparent without labeling individual neurons. Given the implied role for visual landmark learning in *Heliconius* foraging behavior (Jones, 1930; Gilbert, 1972, 1975; Mallet, 1986), we hypothesise that their massively expanded mushroom body supports an integration of visual information.

In other species the mushroom body also receives gustatory and mechanosensory input (Schildberger, 1983; Homberg, 1984; Li and Strausfeld, 1999; Farris, 2008). These may also be of relevance in *Heliconius* given the importance of gustatory and mechanosensory reception in host-plant identification (Schoonhoven, 1968; Renwick and Chew, 1994; Briscoe et al., 2013) and pollen loading (Krenn and Penz, 1998; Penz and Krenn, 2000), although it should be noted that there is currently no evidence these behaviors are learnt (Kerpel and Moreira, 2005; Salcedo, 2011; Silva et al., 2014).

Potential cellular changes associated with ontogenetic mushroom body expansion

The cellular basis of ontogenetic and environmentally induced plasticity may provide further clues as to the functional changes associated with mushroom body expansion during *Heliconius* evolution. The volumetric changes we observe must reflect differences in cell numbers and/or branching and connectivity. It is unknown whether KC neurogenesis is restricted to the larval and pupal stages in Lepidoptera, as it is in Hymenoptera (Fahrbach et al., 1995) where post-eclosion expansion results solely from increased neurite branching (Gronenberg et al., 1996; Farris et al., 2001). In Hymenoptera, age-dependent expansion of the MB-ca accompanies growth of extrinsic neuron processes, whilst increased branching complexity of KCs is associated experience-dependent expansion and foraging specialization in social castes (Farris et al., 2001; Jones et al., 2009). This suggests that changes in the calyx circuitry involving increased synaptic connections onto KC dendrites may be responsible for the volumetric changes associated with behavioral experience. Although we have not yet measured KC number or dendritic branch length, the grade-shifts of MB-ca and MB-lo over MB-pe, that are uncovered by our allometric

738 analyses, indicate that post-eclosion growth is not solely (if at all) due to additional
739 KCs. This is because each additional KC will necessarily contribute volume to all
740 three major MB compartments, MB-ca, MB-pe and MB-lo. Indeed, Ott and Rogers
741 (2010) proposed that wiring overheads might increase non-linearly with increasing
742 KC numbers to explain the positive allometric scaling of MB-ca over MB-lo observed
743 in some other insects. The resultant scaling need not be isometric, however, this effect
744 will always produce a constant allometric scaling relationship. In contrast, the grade-
745 shifts we observe are most likely explained by increased dendritic growth and
746 connectivity in the MB-ca and MB-lo. Confirming this interpretation, and
747 understanding its functional relevance, may provide some insight into how
748 environmental information is stored during post-eclosion development.
749
750 ***Conclusions***
751 Our volumetric analyses uncover extensive phylogenetic expansion and ontogenetic
752 plasticity of *Heliconius* mushroom bodies. Both processes may be linked to the
753 derived foraging behavior or this genus, which relies on allocentric memory of pollen
754 resources (Gilbert, 1975; Sivinski, 1989). This hypothesis must now be confirmed in
755 wider comparative analyses and tested explicitly in behavioral experiments. Our
756 phenotypic observations furthermore provide the necessary framework for analyses of
757 the underpinning neuronal mechanisms regulating neuropil size, and of the
758 consequences for circuit function.
759
760 ## Acknowledgments
761 The authors are grateful to Adriana Tapia, Moises Abanto, William Wcislo, Owen
762 McMillan, Chris Jiggins, and the Smithsonian Tropical Research Institute for
763 assistance, advice, and the use of the *Heliconius* insectaries at Gamboa, Panama, and
764 the Ministerio del Ambiente for permission to collect butterflies in Panama. We also
765 thank Judith Mank's research group at UCL for helpful advice and feedback, and the
766 UCL Imaging Facility for help with confocal microscopy.
767
768 ## Conflict of interest statement
769 The authors declare no conflict of interest.
770

Role of authors

All authors read and approved the final manuscript. Study conception: SHM. Study design and preliminary experiments: SHM, RMM, SRO. Fieldwork and insectary rearing: SHM, RMM. Acquisition of data, analysis, interpretation and initial manuscript draft: SHM. Final interpretation and drafting: SHM, RMM, SRO.

Literature cited

Barton RA. 1998. Visual specialization and brain evolution in primates. Proc Biol Sci 265:1933–1937.

Barton RA, Purvis A, Harvey PH. 1995. Evolutionary radiation of visual and olfactory brain systems in primates, bats and insectivores. Philos Trans R Soc Lond B Biol Sci 348:381–92.

Beltrán M, Jiggins CD, Brower AVZ, Bermingham E, Mallet J. 2007. Do pollen feeding , pupal-mating and larval gregariousness have a single origin in *Heliconius* butterflies: Inferences from multilocus DNA sequence data. :221–239.

Benson WW. 1972. Natural selection for Miillerian mimicry in *Heliconius erato* in Costa Rica. Science (80) 176:936–939.

Berg BG, Galizia CG, Brandt R, Mustaparta H. 2002. Digital atlases of the antennal lobe in two species of tobacco budworm moths, the Oriental *Helicoverpa assulta* (male) and the American *Heliothis virescens* (male and female). J Comp Neurol 446:123–134.

Boeckh J, Boeckh V. 1979. Threshold and odor specificity of pheromone-sensitive neurons in the deutocerebrum of *Antheraea pernyi* and *A. polyphemus* (Saturnidae). J Comp Physiol A 132:235–242.

Boggs CL, Smiley JT, Gilbert LE. 1981. Patterns of pollen exploitation by *Heliconius* butterflies. Oecologia 48:284–289.

Brandt R, Rohlfing T, Rybak J, Krofczik S, Maye A, Westerhoff M, Hege H-C, Menzel R. 2005. Three-dimensional average-shape atlas of the honeybee brain and its applications. J Comp Neurol 492:1–19.

Briscoe AD, Macias-Muñoz A, Kozak KM, Walters JR, Yuan F, Jamie GA, Martin SH, Dasmahapatra KK, Ferguson LC, Mallet J, Jacquin-Joly E, Jiggins CD. 2013. Female behaviour drives expression and evolution of gustatory receptors in butterflies. PLoS Genet 9:e1003620.

Brown KS. 1981. The biology of *Heliconius*. Annu Rev Entomol 26:427–457.

806 Capaldi EA, Robinson GE, Fahrback SE. 1999. Neuroethology of spatial learning: the
807 birds and the bees. Annu Rev Psychol 50:651–682.

808 Cardoso MZ, Gilbert LE. 2013. Pollen feeding, resource allocation and the evolution
809 of chemical defence in passion vine butterflies. J Evol Biol 26:1254–60.

810 Carlsson MA, Schäpers A, Nässel DR, Janz N. 2013. Organization of the olfactory
811 system of nymphalidae butterflies. Chem Senses 38:355–67.

812 Chittka L, Niven J. 2009. Are Bigger Brains Better? Curr Biol 19:R995–R1008.

813 Cohen J. 1988. Statistical power analysis for the behavioral sciences. 2nd ed.
814 Hillsdale, NJ.: Lawrence Earlbaum Associates.

815 Dasmahapatra KK, Walters JR, Briscoe AD, Davey JW, Whibley A, Nadeau NJ,
816 Zimin AV, Hughes DST, Ferguson LC, Martin SH, Salazar C, Lewis JJ, Adler S,
817 Ahn S-J, Baker DA, Baxter SW, Chamberlain NL, Chauhan R, Counterman BA,
818 Dalmay T, Gilbert LE, Gordon K, Heckel DG, Hines HM, Hoff KJ, Holland
819 PWH, Jacquin-Joly E, Jiggins FM, Jones RT, Kapan DD, Kersey P, Lamas G,
820 Lawson D, Mapleson D, Maroja LS, Martin A, Moxon S, Palmer WJ, Papa R,
821 Papanicolaou A, Pauchet Y, Ray DA, Rosser N, Salzberg SL, Supple MA,
822 Surridge A, Tenger-Trolander A, Vogel H, Wilkinson PA, Wilson D, Yorke JA,
823 Yuan F, Balmuth AL, Eland C, Gharbi K, Thomson M, Gibbs RA, Han Y,
824 Jayaseelan JC, Kovar C, Mathew T, Muzny DM, Ongeri F, Pu L-L, Qu J,
825 Thornton RL, Worley KC, Wu Y-Q, Linares M, Blaxter ML, Ffrench-Constant
826 RH, Joron M, Kronforst MR, Mullen SP, Reed RD, Scherer SE, Richards S,
827 Mallet J, Owen McMillan W, Jiggins CD. 2012. Butterfly genome reveals
828 promiscuous exchange of mimicry adaptations among species. Nature 487:94–8.

829 Dreyer D, Vitt H, Dippel S, Goetz B, El Jundi B, Kollmann M, Huetteroth W,
830 Schachtner J. 2010. 3D standard brain of the Red Flour Beetle *Tribolium*
831 *castaneum*: A tool to study metamorphic development and adult plasticity. Front
832 Syst Neurosci 4:3.

833 Dunlap-Pianka H, Boggs CL, Gilbert LE. 1977. Ovarian dynamics in heliconiine
834 butterflies: programmed senescence versus eternal youth. Science (80) 197:487–
835 490.

836 Durst C, Eichmüller S, Menzel R. 1994. Development and experience lead to
837 increased volume of subcompartments of the honeybee mushroom body. Behav
838 Neural Biol 62:259–263.

839 Edgar RC. 2004. MUSCLE: multiple sequence alignment with high accuracy and
840 high throughput. Nucleic Acids Res 32:1792–7.

841 Ehrlich PR, Gilbert LE. 1973. Population Structure and dynamics of the Tropical
842 butterfly *Heliconius ethilla*. Biotropica 5:69–82.

843 Estrada C, Jiggins CD. 2002. Patterns of pollen feeding and habitat preference among
844 Heliconius species. Ecol Entomol 27:448–456.

845 Fahrbach SE, Farris SM, Sullivan JP, Robinson GE. 2003. Limits on volume changes
846 in the mushroom bodies of the honeybee brain. J Neurobiol 57:141–151.

847 Fahrbach SE, Giray T, Robinson GE. 1995. Volume changes in the mushroom bodies
848 of adult honey bee queens. Neurobiol Learn Mem 63:181–191.

849 Fahrbach SE, Moore D, Capaldi E a., Farris SM, Robinson GE. 1998. Experience-
850 expectant plasticity in the mushroom bodies of the honeybee. Learn Mem 5:115–
851 123.

852 Farris SM, Roberts NS. 2005. Coevolution of generalist feeding ecologies and
853 gyrencephalic mushroom bodies in insects. Proc Natl Acad Sci U S A
854 102:17394–17399.

855 Farris SM, Robinson GE, Fahrbach SE. 2001. Experience- and age-related outgrowth
856 of intrinsic neurons in the mushroom bodies of the adult worker honeybee. J
857 Neurosci 21:6395–6404.

858 Farris SM, Schulmeister S. 2011a. Parasitoidism, not sociality, is associated with the
859 evolution of elaborate mushroom bodies in the brains of hymenopteran insects.
860 Proc Biol Sci 278:940–951.

861 Farris SM. 2005. Evolution of insect mushroom bodies: Old clues, new insights.
862 Arthropod Struct Dev 34:211–234.

863 Farris SM. 2008. Tritocerebral tract input to the insect mushroom bodies. Arthropod
864 Struct Dev 37:492–503.

865 Farris SM. 2013. Evolution of complex higher brain centers and behaviors: behavioral
866 correlates of mushroom body elaboration in insects. Brain Behav Evol 82:9–18.

867 Finkbeiner SD. 2014. Communal roosting in heliconius butterflies (Nymphalidae):
868 roost recruitment, establishment, fidelity, and resource use trends based on age
869 and sex. J Lepid Soc 68:10–16.

870 Gilbert LE. 1972. Pollen feeding and reproductive biology of *Heliconius* butterflies.
871 Proc Natl Acad Sci U S A 69:1403–1407.

872 Gilbert LE. 1975. Ecological consequences of a coevolved mutualism between
873 butterflies and plants. In: Gilbert LE, Raven P, editors. Coevolution of animals
874 and plants. p 210–240.

875 Gilbert LE. 1993. An evolutionary food web and its relationship to Neotropical
876 biodiversity. In: Barthlott W, Naumann CM, Schmidt-Loske K, Schuchmann
877 KL, editors. Animal-Plant Interactions in Tropical Environments. Zoologisches
878 Forschungsinstitut und Museum Alexander Koenig, Bonn, Germany. p 17–28.

879 Godenschwege T a., Reisch D, Diegelmann S, Eberle K, Funk N, Heisenberg M,
880 Hoppe V, Hoppe J, Klagges BRE, Martin JR, Nikitina E a., Putz G, Reifegerste
881 R, Reisch N, Rister J, Schaupp M, Scholz H, Schwärzel M, Werner U, Zars TD,

882 Buchner S, Buchner E. 2004. Flies lacking all synapsins are unexpectedly
883 healthy but are impaired in complex behaviour. Eur J Neurosci 20:611–622.

884 Greenacre MJ. 2010. Biplots in practice. Fundacion BBVA.

885 Gronenberg W, Heeren S, Hölldobler B. 1996. Age-dependent and task-related
886 morphological changes in the brain and the mushroom bodies of the ant
887 *Camponotus floridanus*. J Exp Biol 199:2011–9.

888 Gronenberg W, Hölldobler B. 1999. Morphologic representation of visual and
889 antennal information in the ant brain. J Comp Neurol 412:229–240.

890 Gronenberg W. 2001. Subdivisions of hymenopteran mushroom body calyces by their
891 afferent supply. J Comp Neurol 435:474–489.

892 Heinrich B. 1979. Resource heterogeneity and patterns of movement in foraging
893 bumblebees. Oecologia 40:235–245.

894 Heinze S, Florman J, Asokaraj S, El Jundi B, Reppert SM. 2013. Anatomical basis of
895 sun compass navigation II: the neuronal composition of the central complex of
896 the monarch butterfly. J Comp Neurol 521:267–98.

897 Heinze S, Reppert SM. 2012b. Anatomical basis of sun compass navigation I: the
898 general layout of the monarch butterfly brain. J Comp Neurol 520:1599–628.

899 Hofbauer A, Ebel T, Waltenspiel B, Oswald P, Chen Y, Halder P, Biskup S,
900 Lewandrowski U, Winkler C, Sickmann A, Buchner S, Buchner E. 2009. The
901 Wuerzburg hybridoma library against *Drosophila* brain. J Neurogenet 23:78–91.

902 Homberg U. 1984. Processing of antennal information in extrinsic mushroom body
903 neurons of the bee brain. J Comp Physiol A Neuroethol Sens Neural Behav
904 Physiol:825–836.

905 Huber R, van Staaden MJ, S K Les, Liem KF. 1997. Microhabitat use, trophic
906 patterns, and the evolution of brain structure in African Cichlids. Brain Behav
907 Evol 50:167–182.

908 Huetteroth W, Schachtner J. 2005. Standard three-dimensional glomeruli of the
909 *Manduca sexta* antennal lobe: a tool to study both developmental and adult
910 neuronal plasticity. Cell Tissue Res 319:513–24.

911 Janzen ADH. 1971. Euglossine bees as long-distance pollinators of Tropical plants.
912 Science (80) 171:203–205.

913 Jones BM, Leonard AS, Papaj DR, Gronenberg W. 2013. Plasticity of the worker
914 bumblebee brain in relation to age and rearing environment. Brain Behav Evol
915 82:250–261.

916 Jones F. 1930. The sleeping heliconias of Florida. Nat Hist 30:635–644.

917 Jones TA, Donlan NA, O'Donnell S. 2009. Growth and pruning of mushroom body
918 Kenyon cell dendrites during worker behavioral development in the paper wasp,
919 *Polybia aequatorialis* (Hymenoptera: Vespidae). Neurobiol Learn Mem 92:485–
920 495.

921 El Jundi B, Huetteroth W, Kurylas AE, Schachtner J. 2009. Anisometric brain
922 dimorphism revisited: Implementation of a volumetric 3D standard brain in
923 *Manduca sexta*. J Comp Neurol 517:210–25.

924 Kazawa T, Namiki S, Fukushima R, Terada M, Soo K, Kanzaki R. 2009. Constancy
925 and variability of glomerular organization in the antennal lobe of the silkmoth.
926 Cell Tissue Res 336:119–36.

927 Kerpel SM, Moreira GRP. 2005. Absence of learning and local specialization on host
928 plant selection by *Heliconius erato*. J Insect Behav 18:433–452.

929 Klagges BR, Heimbeck G, Godenschwege TA, Hofbauer A, Pflugfelder GO,
930 Reifegerste R, Reisch D, Schaupp M, Buchner S, Buchner E. 1996. Invertebrate
931 synapsins: a single gene codes for several isoforms in *Drosophila*. J Neurosci
932 16:3154–65.

933 Kozak KM, Wahlberg N, Dasmahapatra KK, Mallet J, Jiggins CD. 2015. Multilocus
934 species trees show the recent adaptive radiation of the mimetic *Heliconius*
935 butterflies. Syst Biol. 64 (3): 505-524.

936 Krenn HW, Penz CM. 1998. Mouthparts of *Heliconius* butterflies (Lepidoptera :
937 Nymphalidae): A search for anatomical adaptations to pollen-feeding behavior.
938 Int J Insect Morphol Embryol 27:301–309.

939 Kühn-Bühlmann S, Wehner R. 2006. Age-dependent and task-related volume changes
940 in the mushroom bodies of visually guided desert ants, *Cataglyphis bicolor*. J
941 Neurobiol 66:511–521.

942 Kurylas AE, Rohlfing T, Krofczik S, Jenett A, Homberg U. 2008. Standardized atlas
943 of the brain of the desert locust, *Schistocerca gregaria*. Cell Tissue Res
944 333:125–45.

945 Kvello P, Løfaldli BB, Rybak J, Menzel R, Mustaparta H. 2009. Digital, three-
946 dimensional average shaped atlas of the *Heliothis virescens* brain with integrated
947 gustatory and olfactory neurons. Front Syst Neurosci 3:14.

948 Lent DD, Pinter M, Strausfeld NJ. 2007. Learning with half a brain. Dev Neurobiol
949 67:740–751.

950 Li Y, Strausfeld NJ. 1999. Multimodal efferent and recurrent neurons in the medial
951 lobes of cockroach mushroom bodies. J Comp Neurol 409:647–63.

952 Maleszka J, Barron AB, Helliwell PG, Maleszka R. 2009. Effect of age, behaviour
953 and social environment on honey bee brain plasticity. J Comp Physiol A
954 Neuroethol Sensory, Neural, Behav Physiol 195:733–740.

955 Mallet J. 1980. A laboratory study of gregarious roosting in the butterfly *Heliconius*
956 *melpomene*. MSc Thesis, University of Newcastle-upon-Tyne.

957 Mallet J. 1986. Gregarious roosting and home range in *Heliconius* butterflies. Natl
958 Geogr Res. 2(2): 198-215

959 Masante-Roca I, Gadenne C, Anton S. 2005. Three-dimensional antennal lobe atlas of
960 male and female moths, *Lobesia botrana* (Lepidoptera: Tortricidae) and
961 glomerular representation of plant volatiles in females. J Exp Biol 208:1147–59.

962 Menzel R. 2014. The insect mushroom body, an experience-dependent recoding
963 device. J Physiol Paris 108:84–95.

964 Mizunami M, Weibrecht JM, Strausfeld NJ. 1998. Mushroom bodies of the
965 cockroach: Their participation in place memory. J Comp Neurol 402:520–537.

966 Montgomery SH, Ott SR. 2015. Brain composition in *Godyris zavaleta* , a diurnal
967 butterfly, Reflects an increased reliance on olfactory information. J Comp Neurol
968 523:869–891.

969 Murawski DA, Gilbert LE. 1986. Pollen flow in *Psiguria warscewiczii*: a comparison
970 of *Heliconius* butterflies and hummingbirds. Oecologia 68:161–167.

971 Van Nouhuys S, Kaartinen R. 2008. A parasitoid wasp uses landmarks while
972 monitoring potential resources. Proc Biol Sci 275:377–385.

973 O'Brien DM, Boggs CL, Fogel ML. 2003. Pollen feeding in the butterfly *Heliconius*
974 *charitonia*: isotopic evidence for essential amino acid transfer from pollen to
975 eggs. Proc Biol Sci 270:2631–2636.

976 Ott SR, Rogers SM. 2010. Gregarious desert locusts have substantially larger brains
977 with altered proportions compared with the solitarious phase. Proc Biol Sci
978 277:3087–96.

979 Ott SR. 2008. Confocal microscopy in large insect brains: zinc-formaldehyde fixation
980 improves synapsin immunostaining and preservation of morphology in whole-
981 mounts. J Neurosci Methods 172:220–30.

982 Pagel M. 1999. Inferring the historical patterns of biological evolution. Nature
983 401:877–84.

984 Penz CM, Krenn HW. 2000. Behavioral adaptations to pollen-Feeding in *Heliconius*
985 butterflies (Nymphalinae, Heliconiinae): An experiment using *Lantana* flowers.
986 J Insect Behav 13 :865–880.

987 Pfeiffer K, Homberg U. 2014. Organization and functional roles of the central
988 complex in the insect brain. Annu Rev Entomol 59:165–84.

989 Rein K, Zöckler M, Mader MT, Grübel C, Heisenberg M. 2002. The *Drosophila*
990 standard brain. Curr Biol 12:227–31.

991 Renwick JAA, Chew FS. 1994. Oviposition behavior in Lepidoptera. Annu Rev
992 Entomol 39:377–400.

993 Rø H, Müller D, Mustaparta H. 2007. Anatomical organization of antennal lobe
994 projection neurons in the moth *Heliothis virescen*s. J Comp Neurol 500:658–75.

995 Rosenheim J a. 1987. Host location and exploitation by the cleptoparasitic wasp
996 *Argochrysis armilla*: the role of learning (Hymenoptera: Chrysididae). Behav
997 Ecol Sociobiol 21:401–406.

998 Rospars JP. 1983. Invariance and sex-specific variations of the glomerular
999 organization in the antennal lobes of a moth, *Mamestra brassicae*, and a
1000 butterfly, Pieris brassicae. J Comp Neurol 220:80–96.

1001 Salcedo C. 2011. Pollen preference for *Psychotria* sp. is not learned in the passion
1002 flower butterfly, *Heliconius erato*. J Insect Sci 11:25.

1003 Schildberger K. 1983. Local interneurons associated with the mushroom bodies and
1004 the central body in the brain of *Acheta domesticus*. Cell Tissue Res 230:573–
1005 586.

1006 Schoonhoven LM. 1968. Chemosensory bases of host plant eelection. Annu Rev
1007 Entomol 13:115–136.

1008 Silva AK, Gonçalves GL, Moreira GRP. 2014. Larval feeding choices in heliconians:
1009 Induced preferences are not constrained by performance and host plant
1010 phylogeny. Anim Behav 89:155–162.

1011 Sivan E, Kopell N. 2004. Mechanism and circuitry for clustering and fine
1012 discrimination of odors in insects. Proc Natl Acad Sci U S A 101:17861–17866.

1013 Sivinski J. 1989. Mushroom body development in nymphalid butterflies: A correlate
1014 of learning? J Insect Behav 2:277–283.

1015 Sjöholm M, Sinakevitch I, Ignell R, Strausfeld NJ, Hansson BS. 2005. Organization
1016 of Kenyon cells in subdivisions of the mushroom bodies of a lepidopteran insect.
1017 J Comp Neurol 491:290–304.

1018 Skiri HT, Rø H, Berg BG, Mustaparta H. 2005. Consistent organization of glomeruli
1019 in the antennal lobes of related species of heliothine moths. J Comp Neurol
1020 491:367–80.

1021 Smith AR, Seid M a, Jiménez LC, Wcislo WT. 2010. Socially induced brain
1022 development in a facultatively eusocial sweat bee *Megalopta genalis*
1023 (Halictidae). Proc Biol Sci 277:2157–2163.

1024 Snell-Rood EC, Papaj DR, Gronenberg W. 2009. Brain size: a global or induced cost
1025 of learning? Brain Behav Evol 73:111–28.

1026 Strausfeld NJ, Sinakevitch I, Brown SM, Farris SM. 2009. Ground plan of the insect
1027 mushroom body: functional and evolutionary implications. J Comp Neurol
1028 513:265–91.

1029 Strausfeld NJ. 2002. Organization of the honey bee mushroom body: Representation
1030 of the calyx within the vertical and gamma lobes. J Comp Neurol 450:4–33.

1031 Tamura K, Peterson D, Peterson N, Stecher G, Nei M, Kumar S. 2011. MEGA5:
1032 molecular evolutionary genetics analysis using maximum likelihood,
1033 evolutionary distance, and maximum parsimony methods. Mol Biol Evol
1034 28:2731–9.

1035 Trautwein MD, Wiegmann BM, Beutel R, Kjer KM, Yeates DK. 2012. Advances in
1036 insect phylogeny at the dawn of the postgenomic era. Annu Rev Entomol
1037 57:449–468.

1038 Turner JRG. 1971. Experiments on the demography of tropical butterflies. II.
1039 Longevity and home-range behaviour in *Heliconius erato*. Biotropica 3:21–31.

1040 Turner JRG. 1981. Adaptation and evolution in *Heliconius*: A defense of
1041 NeoDarwinism. Annu Rev Ecol Syst 12:99–121.

1042 Utz S, Huetteroth W, Vomel M, Schachtner J. 2008. Mas-Allatotropin in the
1043 developing antennal lobe of the Sphinx Moth *Manduca sexta*: Distribution, time
1044 course, developmental regulation, and colocalization with other neuropeptides.
1045 Dev Neurobiol 68:123–142.

1046 Warren AD, Davis KJ, Strangeland EM, Pelham JP, Grishin NV. 2013. Illustrated
1047 lists of American butterflies. http://butterfliesofamerica.com

1048 Warton DI, Duursma RA, Falster DS, Taskinen S. 2012. smatr 3: an R package for
1049 estimation and inference about allometric lines. Methods Ecol Evol 3:257–259.

1050 Wei H, el Jundi B, Homberg U, Stengl M. 2010. Implementation of pigment-
1051 dispersing factor-immunoreactive neurons in a standardized atlas of the brain of
1052 the cockroach *Leucophaea maderae*. J Comp Neurol 518:4113–33.

1053 Withers GS, Day NF, Talbot EF, Dobson HEM, Wallace CS. 2008. Experience-
1054 dependent plasticity in the mushroom bodies of the solitary bee *Osmia lignaria*
1055 (Megachilidae). Dev Neurobiol 68:73–82.

1056 Withers GS, Fahrbach SE, Robinson GE. 1993. Selective neuroanatomical plasticity
1057 and division of labour in the honeybee. Nature 364:238–40.

1058 Zars T. 2000. Behavioral functions of the insect mushroom bodies. Curr Opin
1059 Neurobiol 10:790–795.

1060

1061

1062 ## Abbreviations

AL	antennal lobe
aMe	accessory medulla
AN	antennal nerve
AOTu	anterior optic tubercule
CB	central body
CBL	lower central body
CBU	upper central body
CFN	central fibrous neuropil of AL
DMSO	dimethyl suphoxide
Glom	glomeruli
HBS	HEPES-buffered saline
iMe	inner medulla
iRim	inner rim of the lamina
KC	kenyon cell
La	lamina
LAL	lateral accessory lobes
Lo	lobula
LoP	lobula plate
LU	lower unit of AOTu
MB	mushroom body
MB-ca	mushroom body calyx
MB-lo	mushroom body lobes
MB-pe	mushroom body peduncle
MB-lo+pe	mushroom body lobes and peduncle combined
MBr	midbrain
Me	medulla
MGC	macro-glomeruli complex
NGS	normal goat serum
no	noduli
NU	nodule unit of AOTu
oMe	outer medulla
OR	olfactory receptor
OGC	optic glomerular complex
PA	pyrrolizidine alkaloids
PB	protocerebral bridge
PC	principal component
POTu	posterior optic tubercle
rMid	rest of midbrain
SP	strap of AOTu
UU	upper unit of AOTu
ZnFA	Zinc-Formaldehyde solution

1063

1064

Tables

Table 1: Neuropil volumes and body size of A) *H. erato* and B) *H. hecale*

Table 2: Loadings on Principal Components Analysis of the relative size of brain components across six Lepidoptera.

Table 3: Comparisons between old (O) and young (Y) insectary-reared individuals for A) *H. erato* and B) *H. hecale*. *r* is the effect size. DI indicates the group with a higher value of α, β or fitted axis mean.

Table 4: Comparisons between wild caught (W) and old insectary-reared individuals for A) *H. erato* and B) *H. hecale*. *r* is the effect size. DI indicates the group with a higher value of α, β or fitted axis mean.

Table 5: Effects of age (A) and environmental experience (B) on scaling relationships between mushroom body components

Table 1

A) *H. erato*

	wild caught				*old insectary reared*		*young insectary reared*	
	mean (*n* = 10)	**SD**	**Rel. SD (%)**	**% total neuropil**	**mean (*n* = 10)**	**SD**	**mean (*n* = 10)**	**SD**
Body mass (g)	0.093	0.017	19.999	-	0.074	0.014	0.088	0.019
Body length (mm)	23.833	1.426	5.983	-	23.095	1.773	22.671	0.951
Wing span (mm)	71.408	3.278	4.591	-	69.744	4.12	68.786	2.55
La	7.409E+07	1.052E+07	14.192	13.459	6.95E+07	1.61E+07	5.49E+07	1.25E+07
Me	2.396E+08	3.617E+07	15.094	43.523	2.45E+08	2.76E+07	1.90E+08	3.32E+07
aMe	1.633E+05	3.609E+04	22.094	0.030	1.59E+05	4.61E+04	9.77E+04	1.93E+04
Lon	2.630E+07	4.203E+06	15.984	4.777	2.79E+07	2.89E+06	2.07E+07	4.32E+06
LoP	1.393E+07	2.083E+06	14.952	2.531	1.35E+07	2.22E+06	1.04E+07	2.07E+06
OG	1.054E+06	2.400E+05	22.769	0.191	1.05E+06	2.42E+05	8.85E+05	2.26E+05
AL	1.185E+07	2.450E+06	20.671	2.153	1.19E+07	2.49E+06	7.72E+06	1.10E+06
AOTu	2.199E+06	4.535E+05	20.618	0.400	2.26E+06	3.28E+05	1.52E+06	3.27E+05
MB-ca	4.672E+07	9.290E+06	19.886	8.486	4.50E+07	1.22E+07	2.79E+07	5.75E+06
MB-pe	6.043E+06	1.109E+06	18.343	1.098	6.15E+06	1.35E+06	5.57E+06	1.58E+06
MB-lo	2.267E+07	5.812E+06	25.641	4.118	2.17E+07	4.26E+06	1.28E+07	2.31E+06
CBL	3.017E+05	5.189E+04	17.198	0.055	2.83E+05	6.00E+04	2.24E+05	3.81E+04
CBU	1.180E+06	1.788E+05	15.153	0.214	1.17E+06	2.57E+05	8.90E+05	1.36E+05
Nod	2.966E+04	1.146E+04	38.631	0.005	3.09E+04	1.64E+04	3.16E+04	8.46E+03
PB	2.120E+05	4.804E+04	22.658	0.039	1.96E+05	5.04E+04	1.39E+05	2.02E+04
POTu	4.213E+04	9.976E+03	23.681	0.008	4.20E+04	1.43E+04	2.73E+04	7.93E+03
Total midbrain	1.954E+08	3.365E+07	17.222	35.490	2.04E+08	2.70E+07	1.39E+08	2.28E+07

B) *H. hecale*

	wild caught				*old insectary reared*		*young insectary reared*	
	mean (*n* = 10)	**SD**	**Rel. SD (%)**	**% total neuropil**	**mean (*n* = 9)**	**SD**	**mean (*n* = 10)**	**SD**
Body mass (g)	0.163	0.025	15.317	-	0.154	0.046	0.171	0.047
Body length (mm)	29.693	3.097	10.431	-	28.189	3.0631	29.206	2.75
Wing span (mm)	88.129	8.004	9.082	-	80.6	7.134	86.34	8.012
La	9.751E+07	1.826E+07	18.721	13.939	9.39E+07	2.17E+07	9.64E+07	1.50E+07
Me	2.986E+08	5.342E+07	17.888	42.689	2.48E+08	3.81E+07	2.42E+08	3.66E+07
aMe	1.660E+05	2.951E+04	17.782	0.024	1.40E+05	2.80E+04	1.38E+05	3.67E+04
Lon	3.056E+07	5.630E+06	18.422	4.369	2.80E+07	4.64E+06	2.45E+07	5.06E+06
LoP	1.648E+07	2.972E+06	18.031	2.356	1.45E+07	2.45E+06	1.27E+07	2.53E+06
OG	1.099E+06	3.396E+05	30.894	0.157	9.93E+05	2.12E+05	9.24E+05	2.10E+05
AL	1.216E+07	2.056E+06	16.905	1.739	1.09E+07	1.34E+06	9.36E+06	1.59E+06
AOTu	2.572E+06	6.144E+05	23.891	0.368	2.30E+06	4.46E+05	2.02E+06	3.76E+05
MB-ca	5.271E+07	1.611E+07	30.569	7.534	3.60E+07	7.49E+06	2.60E+07	7.48E+06
MB-pe	6.680E+06	1.525E+06	22.834	0.955	5.92E+06	1.30E+06	4.91E+06	1.39E+06
MB-lo	2.421E+07	6.279E+06	25.930	3.461	1.79E+07	3.56E+06	1.32E+07	3.51E+06
CBL	3.109E+05	6.362E+04	20.467	0.044	2.91E+05	7.15E+04	2.47E+05	3.74E+04
CBU	1.093E+06	2.026E+05	18.541	0.156	1.16E+06	2.05E+05	9.65E+05	1.79E+05
Nod	4.207E+04	1.713E+04	40.730	0.006	3.34E+04	8.35E+03	3.06E+04	1.28E+04
PB	2.424E+05	5.657E+04	23.335	0.035	2.00E+05	3.09E+04	1.64E+05	1.75E+04
POTu	4.183E+04	1.257E+04	30.057	0.006	3.74E+04	8.47E+03	3.20E+04	8.27E+03
Total midbrain	2.551E+08	6.253E+07	24.513	36.465	1.82E+08	2.28E+07	1.50E+08	2.25E+07

Table 2

A) Midbrain only

	Loadings	
	Residuals	
Neuropil	**PC1**	**PC2**
AL	-0.981	-0.045
CB L+U	-0.798	0.406
MB-ca	0.962	0.110
MB-lo+pe	0.952	0.231
AOTu	-0.047	0.966

B) Whole neuropil

	Loadings	
	Residuals	
Neuropil	**PC1**	**PC2**
AL	0.761	0.619
CB L+U	0.671	0.670
MB-ca	-0.961	0.212
MB-lo+pe	-0.942	0.222
AOTu	0.811	0.024
Me	0.042	-0.949
Lob	0.920	-0.354
LoP	0.962	-0.167

Table 3

A) *H. erato*

	Volume			Scaling coefficient (β)			Intercept (α)			Major Axis Shift		
	t_{17}	p	r (DI)	LR	p	r (DI)	Wald $\chi 2$	p	r (DI)	Wald $\chi 2$	p	r (DI)
La	2.432	0.026	0.508 (O)	2.019	0.155	-	2.895	0.089	-	13.196	0.000	0.833 (O)
Me	4.118	0.001	0.707 (O)	0.090	0.765	-	1.127	0.288	-	19.405	0.000	1.000 (O)
aME	3.802	0.001	0.678 (O)	3.976	0.046	0.458 (O)	-	-	-	-	-	-
Lob	4.173	0.001	0.711 (O)	0.246	0.620	-	1.587	0.208	-	20.284	0.000	1.000 (O)
LoP	3.266	0.005	0.621 (O)	0.523	0.470	-	3.802	0.051	-	19.034	0.000	1.000 (O)
OG	1.412	0.176	-	0.385	0.535	-	5.694	0.017	0.547 (Y)	10.622	0.001	0.748 (O)
AL	5.080	0.000	0.776 (O)	4.169	0.041	-	0.214	0.644	-	27.584	0.000	1.000 (O)
AOT	5.192	0.000	0.783 (O)	0.109	0.741	-	0.123	0.726	-	26.321	0.000	1.000 (O)
MB-ca	4.050	0.001	0.701 (O)	3.679	0.055	-	1.607	0.205	-	19.177	0.000	1.000 (O)
MB-lo+pe	4.806	0.000	0.759 (O)	0.963	0.326	-	0.373	0.541	-	23.250	0.000	1.000 (O)
CB L+U	3.272	0.004	0.622 (O)	2.364	0.124	-	1.807	0.179	-	16.530	0.000	0.933 (O)
PB	3.169	0.006	0.609 (O)	5.996	0.014	0.562 (O)	-	-	-	-	-	-
POTu	2.772	0.013	0.558 (O)	1.539	0.215	-	4.124	0.042	0.466 (Y)	14.953	0.000	0.887 (O)
Total Mid	4.192	0.001	0.713 (O)	-	-	-	-	-	-	-	-	-
rMid	5.771	0.000	0.814 (O)	-	-	-	-	-	-	-	-	-
Total OL	5.076	0.000	0.776 (O)	-	-	-	-	-	-	-	-	-
Total neuropil	5.153	0.000	0.781 (O)	-	-	-	-	-	-	-	-	-

B) *H. hecale*

	Volume			Scaling coefficient (β)			Intercept (α)			Major Axis Shift		
	t_{18}	p	r (DI)	LR	p	r (DI)	Wald $\chi 2$	p	r (DI)	Wald $\chi 2$	p	r (DI)
La	-0.424	0.677	-	1.866	0.172	-	11.902	0.001	0.771 (Y)	1.043	0.307	-
Me	0.333	0.743	-	0.494	0.482	-	21.674	0.000	1.000 (Y)	1.971	0.160	-
aME	0.238	0.814	-	0.094	0.759	-	3.044	0.081	-	3.088	0.079	-
Lob	1.538	0.141	-	0.002	0.961	-	3.544	0.060	-	4.501	0.034	0.474 (O)
LoP	1.683	0.110	-	0.066	0.797	-	1.577	0.209	-	5.031	0.025	0.502 (O)
OG	0.617	0.545	-	0.266	0.606	-	4.408	0.036	0.470 (Y)	3.045	0.081	-
AL	2.418	0.026	-	1.795	0.180	-	2.396	0.122	-	6.451	0.011	0.570 (O)
AOT	1.496	0.152	-	0.101	0.751	-	2.166	0.141	-	4.656	0.031	0.483 (O)
MB-ca	3.177	0.005	0.599 (O)	0.283	0.595	-	0.104	0.747	-	9.166	0.002	0.677 (O)
MB-lo+pe	2.707	0.014	0.538 (O)	0.147	0.702	-	0.015	0.902	-	7.594	0.006	0.616 (O)
CB L+U	2.218	0.040	0.463 (O)	3.291	0.070	-	0.859	0.354	-	7.221	0.007	0.601 (O)
PB	3.291	0.004	0.613 (O)	1.043	0.307	-	0.172	0.678	-	9.448	0.002	0.687 (O)
POTu	1.494	0.153	-	0.078	0.780	-	0.736	0.391	-	6.292	0.012	0.561 (O)
Total Mid	3.054	0.007	0.584 (O)	-	-	-	-	-	-	-	-	-
rMid	2.854	0.011	0.558 (O)	-	-	-	-	-	-	-	-	-
Total OL	0.280	0.783	-	-	-	-	-	-	-	-	-	-
Total neuropil	1.082	0.293	-	-	-	-	-	-	-	-	-	-

Table 4

A) *H. erato*

	Volume			Scaling coefficient (β)			Intercept (α)			Major Axis Shift		
	t_{17}	p	r (DI)	LR	p	r (DI)	Wald $\chi 2$	p	r (DI)	Wald $\chi 2$	p	r (DI)
La	0.892	0.385	-	3.685	0.055	-	3.605	0.058	-	0.210	0.646	-
Me	-0.426	0.676	-	0.269	0.604	-	2.056	0.152	-	1.269	0.260	-
aME	0.359	0.724	-	5.150	0.023	0.521 (O)	-	-	-	-	-	-
Lob	-1.056	0.306	-	0.283	0.595	-	1.004	0.316	-	1.999	0.157	-
LoP	0.430	0.673	-	4.963	0.026	0.511 (O)	-	-	-	-	-	-
OG	0.116	0.909	-	2.148	0.143	-	2.055	0.152	-	0.848	0.357	-
AL	-0.035	0.972	-	1.695	0.193	-	2.269	0.132	-	0.899	0.343	-
AOT	-0.490	0.631	-	0.483	0.487	-	1.318	0.251	-	1.456	0.227	-
MB-ca	0.511	0.616	-	5.833	0.016	0.554 (O)	-	-	-	-	-	-
MB-lo+pe	0.239	0.814	-	0.714	0.398	-	4.418	0.036	0.482 (W)	7.594	0.006	0.632 (W)
CB L+U	0.394	0.699	-	4.272	0.039	0.474 (O)	-	-	-	-	-	-
PB	0.845	0.410	-	4.413	0.036	0.482 (O)	-	-	-	-	-	-
POTu	0.196	0.847	-	3.726	0.054	-	2.730	0.098	-	0.905	0.341	-
Total Mid	-0.732	0.474	-	-	-	-	-	-	-	-	-	-
rMid	-1.787	0.092	-	-	-	-	-	-	-	-	-	-
Total OL	-0.123	0.904	-	-	-	-	-	-	-	-	-	-
Total neuropil	-0.432	0.671	-	-	-	-	-	-	-	-	-	-

B) *H. hecale*

	Volume			Scaling coefficient (β)			Intercept (α)			Major Axis Shift		
	t_{18}	p	r (DI)	LR	p	r (DI)	Wald $\chi 2$	p	r (DI)	Wald $\chi 2$	p	r (DI)
La	0.437	0.667	-	6.725	0.010	0.580 (O)	-	-	-	-	-	-
Me	2.293	0.034	0.475 (W)	9.165	0.002	0.677 (O)	-	-	-	-	-	-
aME	1.898	0.074	-	3.728	0.054	-	1.463	0.227	-	8.056	0.005	0.688 (W)
Lob	1.017	0.322	-	9.760	0.002	0.699 (O)	-	-	-	-	-	-
LoP	1.609	0.125	-	6.081	0.014	0.551 (O)	-	-	-	-	-	-
OG	0.614	0.547	-	4.262	0.039	0.462 (O)	-	-	-	-	-	-
AL	1.519	0.146	-	7.095	0.008	0.596 (O)	-	-	-	-	-	-
AOT	1.088	0.291	-	3.938	0.047	0.444 (O)	-	-	-	-	-	-
MB-ca	3.126	0.006	0.593 (W)	1.657	0.198	-	0.395	0.530	-	10.432	0.001	0.722 (W)
MB-lo+pe	2.536	0.021	0.513 (W)	3.759	0.053	-	1.603	0.205	-	8.811	0.003	0.664 (W)
CB L+U	-0.446	0.661	-	1.665	0.197	-	11.013	0.001	0.742 (O)	2.385	0.122	-
PB	1.919	0.071	-	5.043	0.025	0.502 (O)	-	-	-	-	-	-
POTu	0.551	0.588	-	5.420	0.020	0.521 (O)	-	-	-	-	-	-
Total Mid	3.658	0.002	0.653 (W)	-	-	-	-	-	-	-	-	-
rMid	3.417	0.003	0.627 (W)	-	-	-	-	-	-	-	-	-
Total OL	1.728	0.101	-	-	-	-	-	-	-	-	-	-
Total neuropil	2.553	0.020	0.516 (W)	-	-	-	-	-	-	-	-	-

Table 5

A) ***Old vs young insectary reared***

		Scaling coefficient (β)			Intercept (α)			Major Axis Shift		
	components	**Likelihood Ratio**	**p**	**r**	**Wald χ2**	**p**	**r**	**Wald χ2**	**p**	**r (DI)**
H. erato	MB ca + lo	0.627	0.428	-	2.249	0.134		16.987	0.000	0.946 (O)
	MB ca + pe	1.224	0.269	-	12.457	0.000	0.810	-	-	-
	MB lo + pe	0.206	0.650	-	29.286	0.000	1.000	-	-	-
H. hecale	MB ca + lo	0.100	0.752	-	0.058	0.810		8.771	0.003	0.662 (O)
	MB ca + pe	0.376	0.540	-	6.422	0.011	0.567	-	-	-
	MB lo + pe	0.118	0.731	-	5.462	0.019	0.523	-	-	-

B) ***Wild vs. old insectary reared***

		Scaling coefficient (β)			Intercept (α)			Major Axis Shift		
	components	**Likelihood Ratio**	**p**	**r**	**Wald χ2**	**p**	**r**	**Wald χ2**	**p**	**r (DI)**
H. erato	MB ca + lo	4.083	0.043	0.464	0.139	0.709	-	0.186	0.667	-
	MB ca + pe	0.311	0.577	-	0.732	0.392	-	0.044	0.834	-
	MB lo + pe	1.296	0.255	-	0.213	0.645	-	0.011	0.916	-
H. hecale	MB ca + lo	0.307	0.580	-	0.398	0.528	-	7.901	0.005	0.629 (W)
	MB ca + pe	2.942	0.086	-	7.340	0.007	0.606	-	-	-
	MB lo + pe	1.553	0.213	-	4.086	0.043	0.452	-	-	-

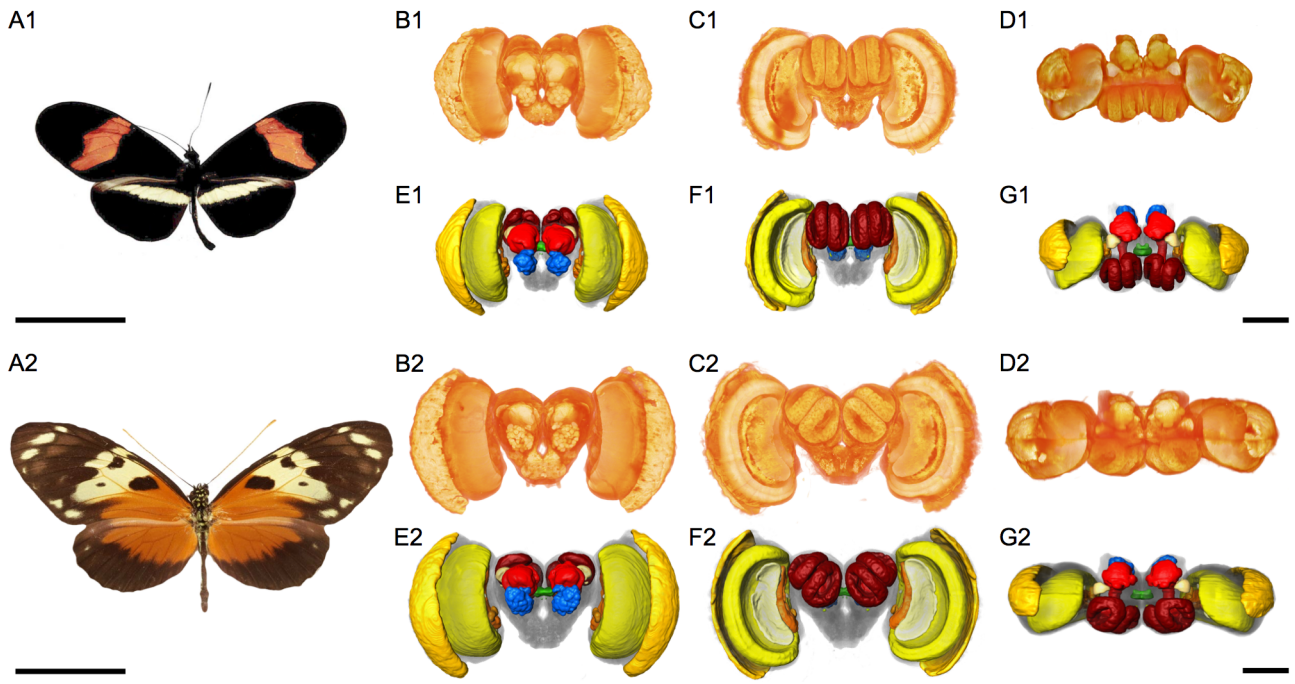

Figure 1: Overview of the anatomy of the Heliconius brain.

3D models of *H. erato* (A1–G1) and *H. hecale* (A2–G2). B1–D1 and B2–D2: Volume rendering of synapsin immunofluorescence showing the surface morphology of the brain neuropil from the anterior (A1/A2), posterior (B1/B2), and dorsal (C1/C2) view. E1–G1 and E2–G2: Surface reconstructions of the major neuropil compartments from the anterior (D1/D2), posterior (E1/E2), and dorsal (F1/F2) view. Neuropil in yellow-orange: visual neuropil, green: central complex, blue: antennal lobes, red: mushroom bodies. See Figures 2–4 for further anatomical detail. The individuals displayed are male. Images in A1/A2 are from Warren et al. (2013). Scale bars = 25 mm in A1/A2; 500 µm in B1–D1/B2–D2.

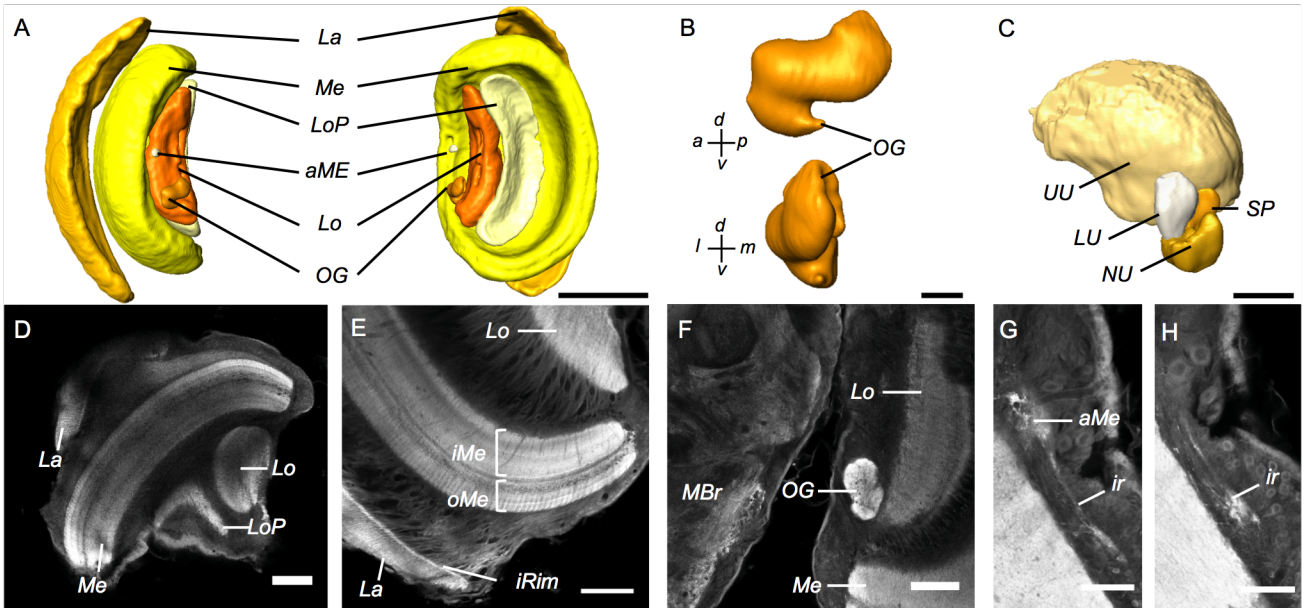

Figure 2: Anatomy of the major visual neuropils.

A: Surface reconstructions of the optic lobe neuropils viewed from anterior (left image) and posterior (right image). They comprise the lamina (La), the medulla (Me), and accessory medulla (aMe), the lobula (Lo), the lobula plate (LoP) and the optic glomerulus (OG). B: Surface reconstruction of the optic glomerulus (OG) viewed along the anterior-posterior axis (top) and an anterior view (bottom). C: Surface reconstruction of the anteriot optic tubercle (AOTu). D–J: Synapsin immunofluorescence in single confocal sections of the optic lobe of H. hecale. D: Horizontal section showing all four major optic lobe neuropils (La, Me, Lo, LoP). E: Frontal section showing the inner rim (iRim) of the lamina, a thin layer on its inner surface that is defined by intense synapsin immunofluorescence. Synapsin immunostaining also reveals the laminated structure of the medulla with two main subdivisions, the outer and inner medulla (oMe, iMe). F: The OG is located medially to the Lo; frontal section, the midbrain (MBr) occupies the left half of the frame. G,H: Frontal sections showing a small, irregular neuropil (ir) observed running from the anterior-ventral boundary of the aME as in *D. plexippus* (Heinze and Reppert, 2012). All images are from male *H. hecale*.

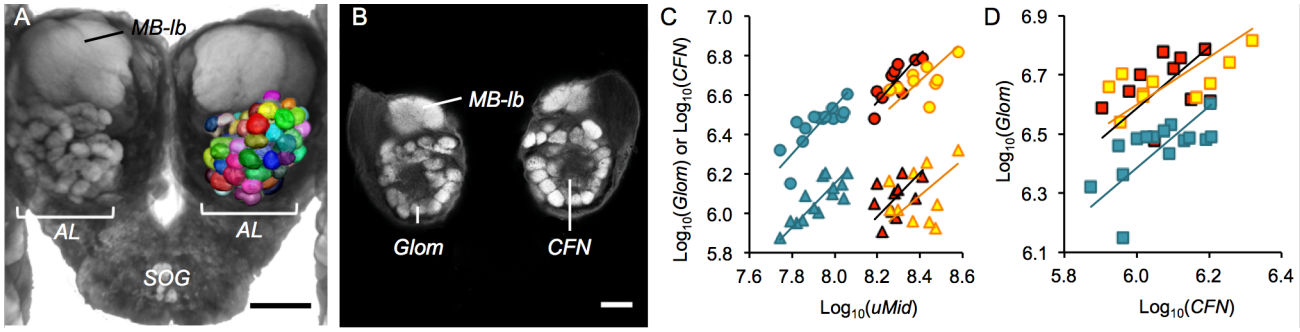

Figure 3: Anatomy of the antennal lobe

A: 3D reconstruction of individual antennal lobe (AL) glomeruli superimposed on a volume rendering of the anterior surface of the midbrain. B: Synapsin immunofluorescence in a single frontal confocal section showing the glomeruli (Glom) surrounding the central fibrous neuropil (CFN). Images A–B are from male *H. hecale*. C,D: Allometric grade-shifts between Glomerular (circles) or CFN (triangles) volume and unsegmented midbrain volume (C), and between Glomerular and CFN volume (D) in *G. zavaleta* (solid blue), *H. erato* (black filled with red) and *H. hecale* (orange filled with yellow). Scale bars = 500 μm in A; 50 μm in B,C,G,H; 100 μm in B–F, J; 200 μm in I.

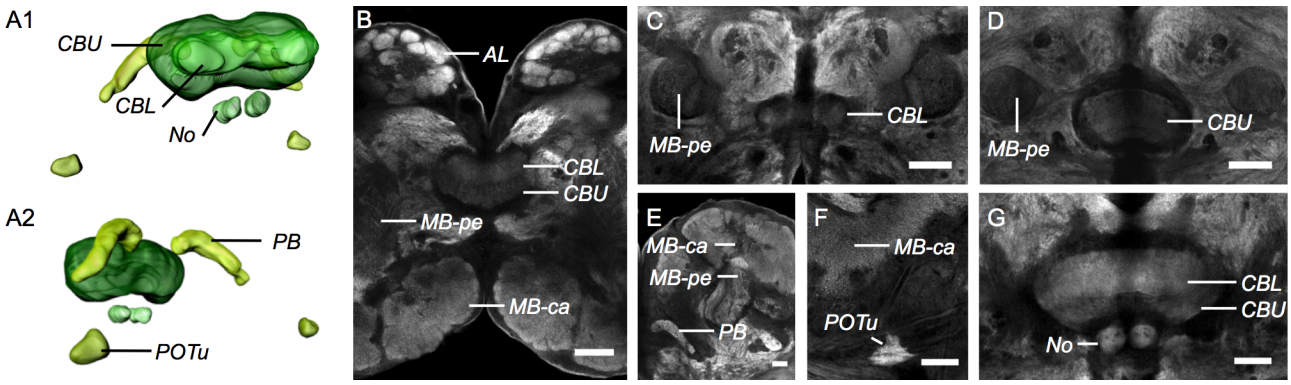

Figure 4: Anatomy of the central complex

A1/A2: Surface reconstruction of the central complex from an anterolateral (A1) and oblique posteroventral (A2) view, showing the upper and lower subunit of the central body (CBU, CBL), the noduli (No), the protocerebral bridge (PB) and posterior optic tubercles (POTu). B–G: Synapsin immunofluorescence in single confocal sections. B: Horizontal section showing the upper and lower subunit of the CB in relation to the antennal lobes (AL) and the calyx (MB-ca) and pedunculus (MB-pe) of the mushroom body. C,D: Frontal confocal sections at the level of the CBL (C) and CBU (D); the CB subunits are flanked by the profiles of the vertically running MB-pe on either side. E: Frontal section showing the location of the PB ventrally to the MB-ca. F: POTu positioned ventrally to the MB-ca in a frontal section. G: Frontal section showing position of the paired No ventrally to CBL and CBU. All images are from a male H. hecale. Scale bars = 100 µm in B–D, G; 50 µm in E,F.

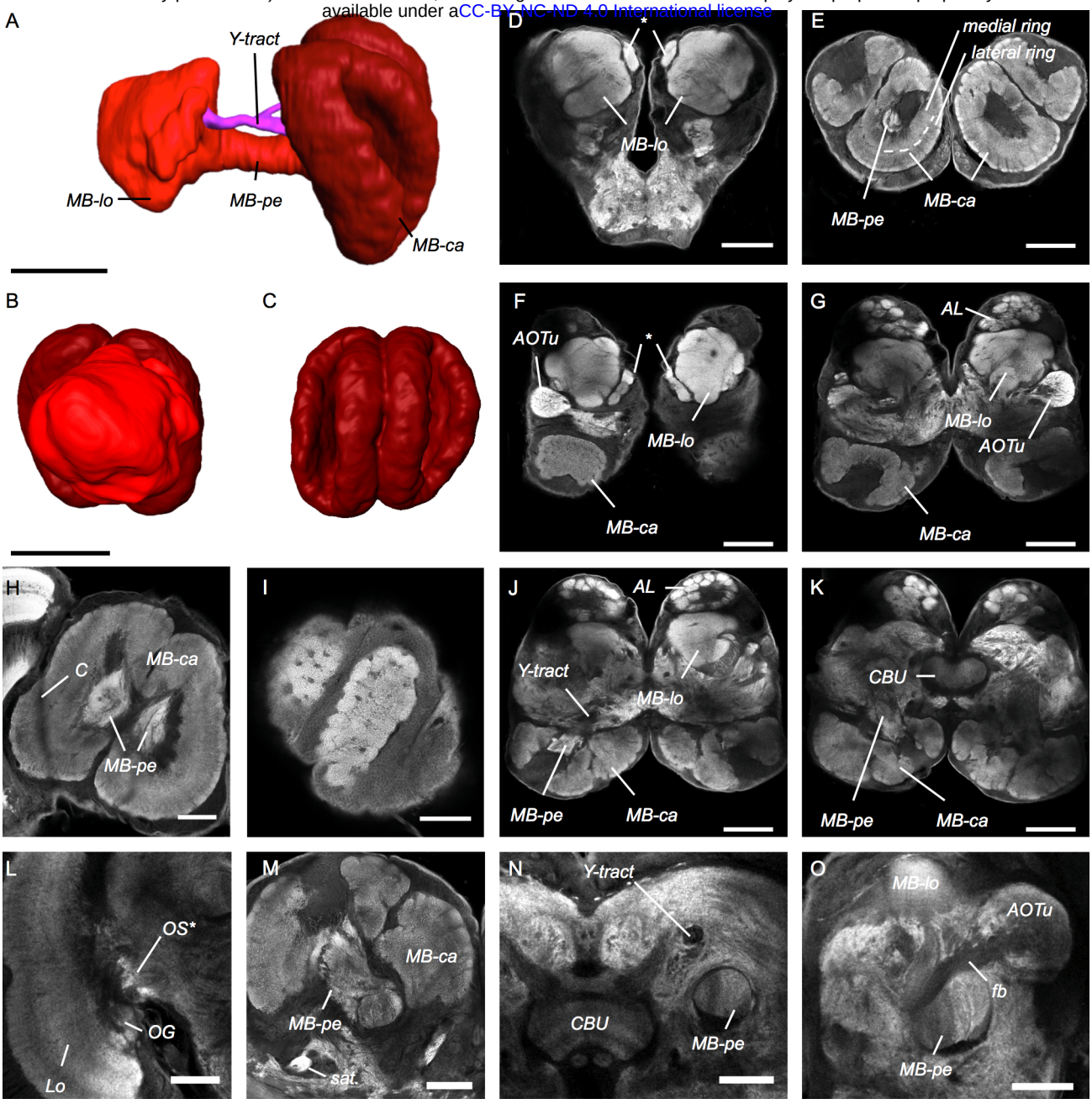

Figure 5: Anatomy of the mushroom body

A–C: Surface reconstruction of the mushroom body viewed orthogonal to the anterior-posterior axis from a medial vantage point level with the peduncle (A); from anterior (B); and from posterior (C). The main components are the calyx (MB-ca) shown in dark red, and the peduncle (MB-pe) and lobes (MB-lo) shown in bright red. A Y-tract, shown in magenta, runs parallel and slightly medial to the MB-pe. D–O: Synapsin immunofluorescence in individual confocal sections. D: anterior view of the midbrain showing the MB-lo, an asterik indicates what is most likely the ventral lobe, otherwise the individual lobes and loblets of the MB-lo are fused. E: Frontal section at a posterior level near the end of the MB-pe, showing the profiles of the MB-ca with its zonation into an outer and a medial ring. F,G and J,K: Horizontal confocal sections through the midbrain at increasing depths from dorsal towards ventral, showing MB structure in relation to neighboring neuropil: the anterior optic tubercle (AOTu in F,G); the antennal lobe (AL in G,J); and the central body upper division (CBU in K). H: An example of a female *H. erato* where the MB-ca is deformed due expansion into the optic lobe and constriction (labeled C) at the optic stalk by the neural sheath surrounding the brain. I: Pitted surface of the MB-ca in a very posterior tangential horizontal section. The pitting is related to what appear to be columnar domains within the calyx neuropil (cf. MB-ca in J,K,M). L: Areas of intense synapsin staining in the optic stalk (OS*); Lo, lobula; OG, optic glomerulus. M: Frontal section near the base of the calyx (MB-ca) showing a satellite neuropil (sat.) located near to the MB-pe. N: A Y-tract runs parallel with, and dorsally and slightly medially to the MB-pe; both are seen in profile in this frontal section. O: A fiber bundle (fb) connected to the AOTu running near the junction between the MB-pe and MB-lo. With the exception of I, all images are from a male *H. hecale*. Scale bars A-G, J-K = 200 µm, H-I, L-O = 100 µm.

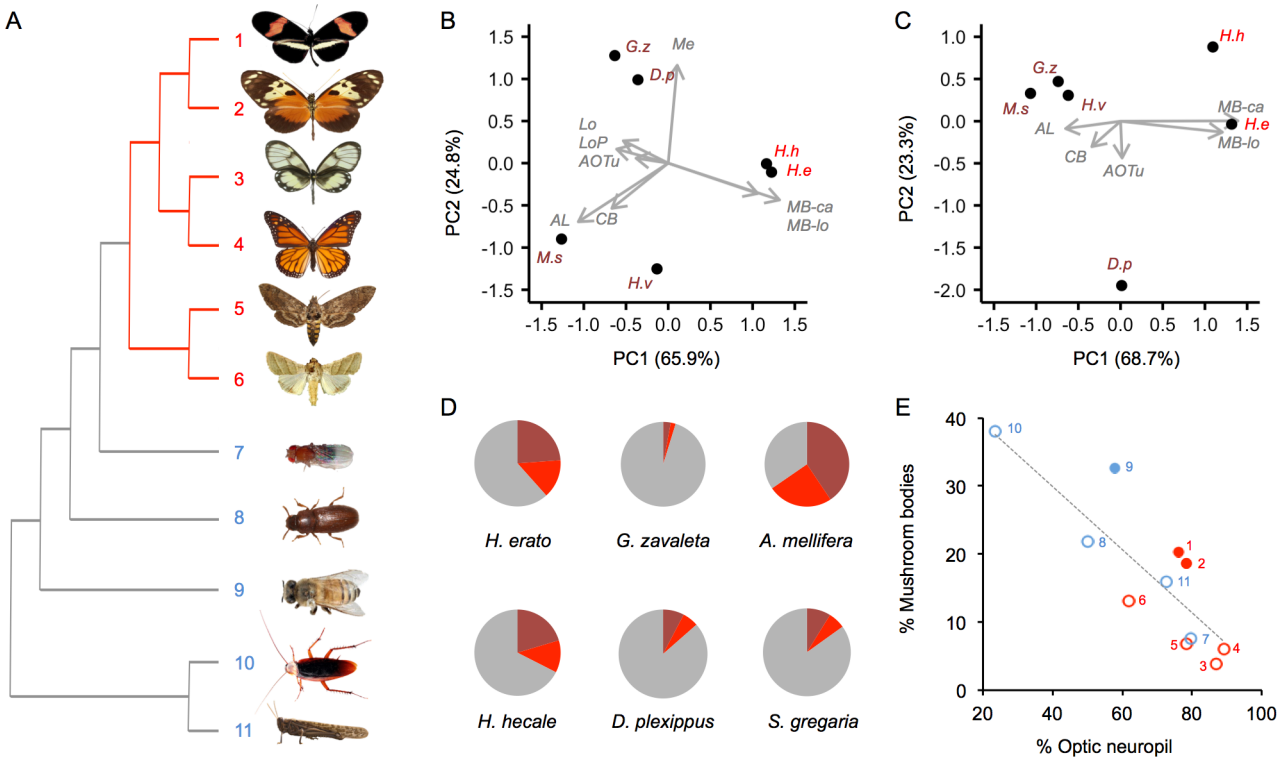

Figure 6: Divergence in brain structure across Lepidoptera, and in mushroom body size across insects.

A: Phylogenetic relationships of Lepidoptera (red branches) and other insects (grey branches) for which directly comparable data are available. Branches are not drawn proportional to divergence dates, numbers refer to labels in panel E. B,C: Principal Component analysis of segmented neuropil volumes, corrected for allometric scaling with the unsegmented midbrain and phylogeny. B shows the results of an analysis using all neuropil. C shows the results of an analysis excluding the optic lobe neuropil. Species data points are indicated by the first letter of their genus and species name: D.p = *Danaus plexippus*; H.e = *Heliconius erato*; H.h = *H. hecale*; G.z = *Godyris zavaleta*; H.v = *Heliothis virescens*; M.s = *Manduca sexta*. D: The proportion of the midbrain occupied by MB-ca (dark red) and MB-lo+pe (light red) in four butterflies, and two other insects with fully comparable data. E: Across a wider sample of insects (shown in A), when expressed as a percentage of total volume of OL, AL, CB and MB, *Apis mellifera* (solid blue) and *Heliconius* (solid red) stand out as having expanded mushroom bodies, correcting for the size of the optic neuropil, compared to other Lepidoptera (unfilled red circles) and other insects (unfilled blue circles). The line was fitted by PGLS. All insect images in A are from Wikimedia commons and were released under the Creative Commons License, except *Heliconius* (see Fig. 1).

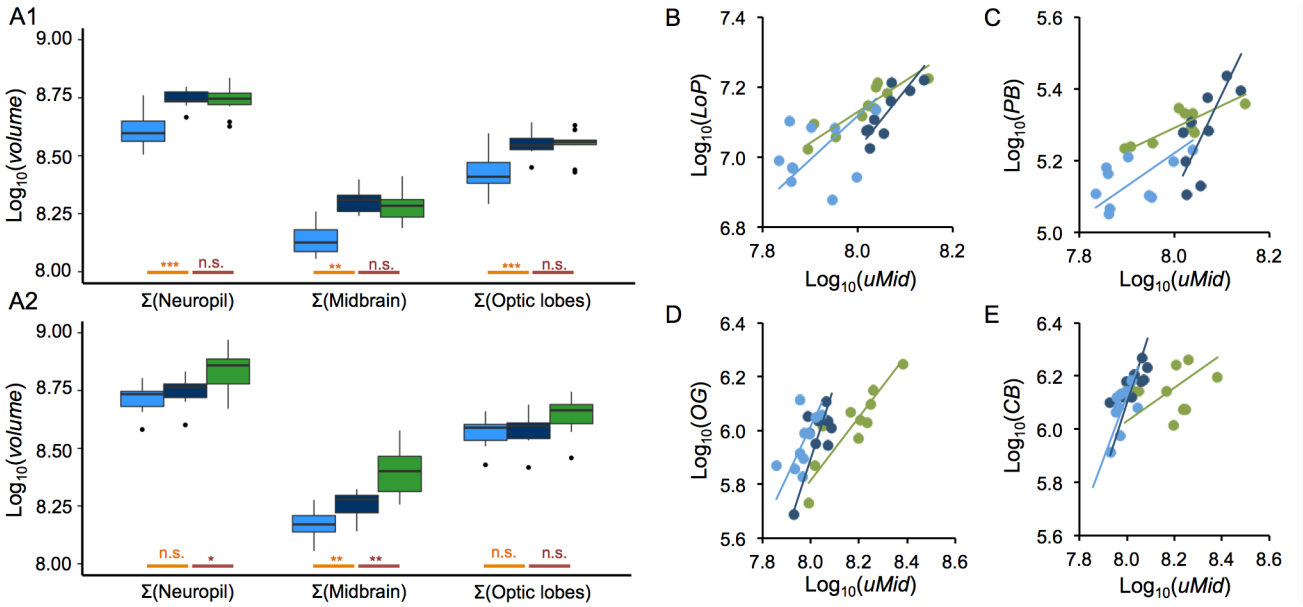

Figure 7: Age and environment dependent growth of brain components

A1,A2: Comparisons of raw volumes of total neuropil, total OL neuropil, total midbrain neuropil between wild-caught, old and young insectary-reared individuals of *H. erato* (A1) and *H. hecale* (A2). Significance of pair-wise comparisons are shown along the x-axis (young-old = orange; old-wild = dark red; n.s. = $p>0.05$, * = $p<0.05$, ** = $p<0.01$, *** = $p<0.001$). B: Allometric scaling of LoP in *H. erato*. C: Allometric scaling of PB in *H. erato*. D: Allometric scaling of OG in *H. hecale*. E: Allometric scaling of CB in *H. hecale*. Note in E and F the shifts in allometry occur along the x-axis, this is explained by the large difference in unsegmented midbrain volume observed between wild-caught and old insectary-reared individuals in *H. hecale* as displayed in D.

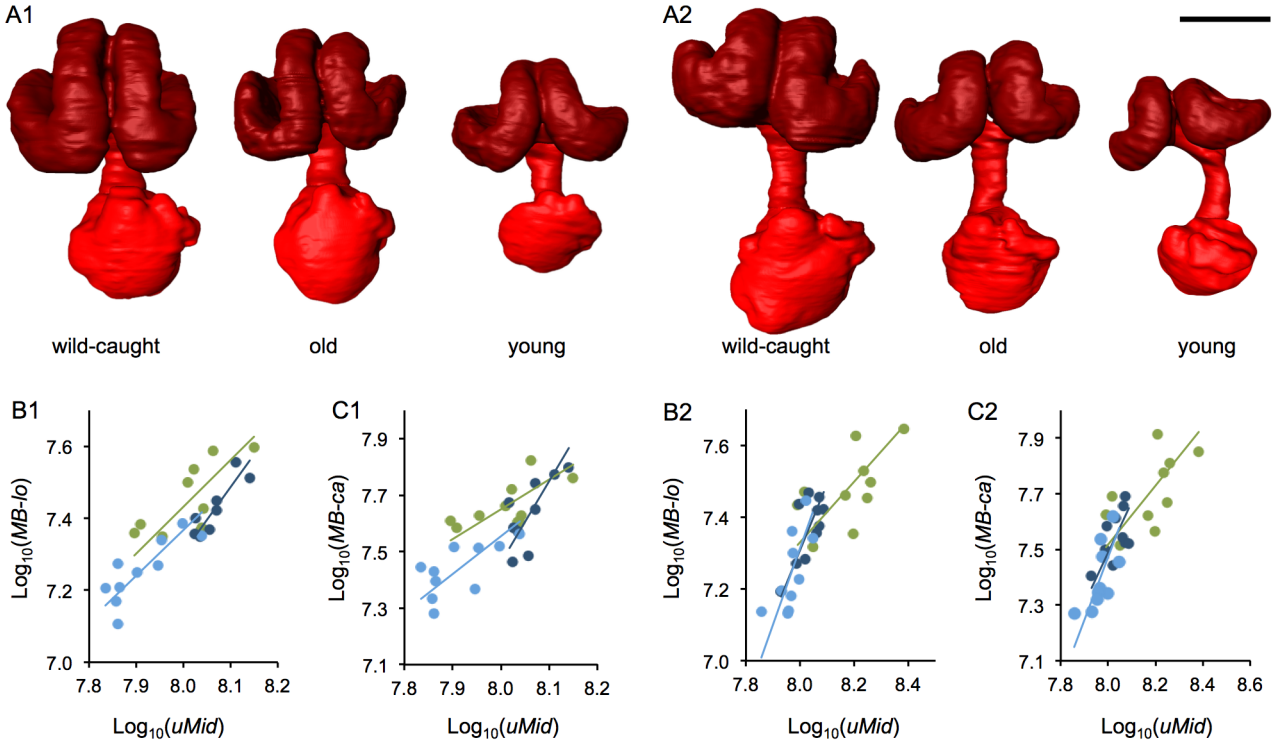

Figure 8: Age and environment dependent growth of the mushroom bodies

Surface reconstruction of the mushroom body viewed along the anterior-posterior axis for wild-caught, old and young insectary-reared individuals of H. erato (A1) and H. hecale (A2). Representative individuals were chosen as those closest to the group mean volume. Scale bar = 200 µm. B1-C1/B2-C2: allometric relationships between MB-lo+pe (B1/B2), or MB-ca (C1/C2),and the volume of the unsegmented midbrain (rMid) for *H. erato* (B1/C1) and *H. hecale* (B2/C2). Data for wild caught individuals are in green, data for old insectary-reared individuals in dark blue, and data for young insectary-reared individuals are in light blue. Allometric slopes for each group are shown, the slope, intercepts and major-axis means are compared in Table 3,4.